CONTRACTOR REPORT

SAND92—7308
IS-5012
Unlimited Release
UC—940

Performance of Sequoyah Containment Anchorage System

Fouad Fanous, Lowell Greimann, Wagdy Wassef, Delwyn Bluhm
Ames Laboratory
Institute for Physical Research and Technology
Iowa State University
Ames, Iowa 50011

Prepared by Sandia National Laboratories Albuquerque, New Mexico 87185
and Livermore, California 94550 for the United States Department of Energy
under Contract DE-AC04-76DP00789

Printed January 1993

Issued by Sandia National Laboratories, operated for the United States Department of Energy by Sandia Corporation.

Available to DOE and DOE contractors from
Office of Scientific and Technical Information
PO Box 62
Oak Ridge, TN 37831

Prices available from (615) 576-8401, FTS 626-8401

Available to the public from
National Technical Information Service
US Department of Commerce
5285 Port Royal Rd
Springfield, VA 22161

NTIS price codes
Printed copy: A04
Microfiche copy: A01

SAND92-7308
IS-5012
Unlimited Release
Printed January 1993

Distribution
Category UC-940

PERFORMANCE OF SEQUOYAH CONTAINMENT ANCHORAGE SYSTEM

Fouad Fanous, Lowell Greimann, Wagdy Wassef, and Delwyn Bluhm
Ames Laboratory
Institute for Physical Research and Technology
Iowa State University
Ames, Iowa 50011

Sandia Project Monitor: M. B. Parks
Work Performed Under Sandia Contract No. 63-6130

Abstract

Deformation of a steel containment anchorage system during a severe accident may result in a leakage path at the containment boundaries. Current design criteria are based on either ductile or brittle failure modes of headed bolts that do not account for factors such as cracking of the containment basemat or deformation of the anchor bolt that may affect the behavior of the containment anchorage system. The purpose of this study was to investigate the performance of a typical ice condenser containment's anchorage system. This was accomplished by analyzing the Sequoyah Containment Anchorage System. Based on a strength of materials approach and assuming that the anchor bolts are resisting the uplift caused by the internal pressure, one can estimate that the failure of the anchor bolts would occur at a containment pressure of 79 psig. To verify these results and to calibrate the strength of materials equation, the Sequoyah containment anchorage system was analyzed with the ABAQUS program using a three-dimensional, finite-element model. The model included portions of the steel containment building, shield building, anchor bolt assembly, reinforced concrete mat and soil foundation material.

As internal pressure was applied, cracks were formed in the vicinity of the anchorage system. Conical failure surfaces were observed at 60 psig. All concrete surrounding the anchor bolt was cracked at 70 psig. At a pressure of 74 psig, a conical surface with a slope of 40 degrees extended to the containment's base plate. Because of convergence problems, the analysis could not be continued beyond this pressure. However, one can hypothesize that if the analysis had continued, enough cracks would probably have occurred to form a complete failure cone above the bottom ring of the anchorage system. This would leave the anchor bolt as the only load transfer mechanism, and hence, inducing large strain with large deformation that may lead to a ductile failure of the anchor bolt.

TABLE OF CONTENTS

LIST OF FIGURES

LIST OF FIGURES (CONTINUED)

ACKNOWLEDGMENT

The authors would like to express their appreciation to Mr. David Clauss and Dr. M. B. Parks from Sandia National Laboratories for their help throughout the course of this work. Special thanks is also extended to Dr. James Costello from the U.S. Nuclear Regulatory Commission and Dr. Walter von Riesemann from Sandia National Laboratories. The authors also wish to thank Mr. Mingche Wu from Iowa State University for his help with the project. Very special thanks is also extended to the Project Secretary, Ms. Connie Bates, for the word processor operations and the secretarial services associated with this project.

EXECUTIVE SUMMARY

Recently, the Containment Technology Division of Sandia National Laboratories has developed methods for predicting the performance of steel containment buildings under pressures that exceed the design values. This method is being employed to estimate the pressure capacity, at elevated temperature, of the Sequoyah containment building shell. To predict shell rupture, Sandia has suggested a failure criterion that is based on the ultimate strain properties of the material and adjusted by knockdown factors. The knockdown factors account for differences between design and actual construction, sophistication of analysis methods, and variations in material property data.

Axisymmetric analyses of the Sequoyah containment have been conducted to determine the global response of the containment shell with local 3-D analyses performed to determine the strain concentrations caused by penetrations. As a continuation of this overall effort to estimate the pressure capacity of the Sequoyah containment, the objective of the present work is to analytically investigate the performance of the anchorage system. The study was carried out using the ABAQUS finite element computer code.

The Sequoyah containment is held down by 180 pretensioned high strength bolts that resist the uplift forces generated by internal pressure or seismic events. Possible failure modes of the containment anchorage system were defined as: (1) ductile failure caused by elongation of the bolts; and, (2) brittle failure caused by failure of the concrete surrounding the bolt. Simplified equations to evaluate the pressures associated with these failure modes are given. However, these equations fail to account for the structural deformation that affects the behavior of the anchorage system, such as deformation of the anchor bolts and its assembly, concrete deformation, cracking of the containment basemat and containment shell deformation.

Because of the complexity involved in estimating the anchorage system behavior, the finite element method was chosen over more classical 'strength of materials' approaches. Analytical modeling of a concrete structure with the finite element method requires consideration of several parameters that influence the predicted behavior of the structure. Bond idealization and shear transfer in cracked concrete were investigated using small concrete models that were tested by others. The finite element analyses showed that the approach employed in the ABAQUS program to idealize these two parameters gave satisfactory results when compared to the test results. Therefore, ABAQUS was selected for analyzing the Sequoyah containment anchorage system.

A one-degree wedge extending between the center of one bolt to midway to the next bolt was idealized for the 3-dimensional nonlinear finite element analysis. The model includes portions of the containment vessel, shield building, anchor bolt, anchorage system, reinforced concrete mat and soil foundation material. Solid and shell elements were used to model the concrete basemat and the steel containment, respectively. The anchor bolt was modeled using beam elements. All interfaces between the steel plates and concrete were idealized using compression-only springs perpendicular to the steel plates. A distributed cracking model was used to represent the mechanical behavior of

concrete in tension. During the analysis, the bolts were first preloaded and then internal pressure loading was applied in discrete steps.

The analysis proceeded without significant convergence problems up to a pressure of 73.8 psig. Beyond this pressure, a load increment of 0.001 psi was used and the analysis continued to a pressure of 74.123 psig. However, numerical problems were encountered when the load was increased beyond this value. ABAQUS personnel were consulted about the problem; however, the source of the problems could not be determined. They suggested using an axisymmetric model for the problem in which the anchor bolt is modeled using axisymmetric elements. The suggestion was considered but rejected since the objective of this work is to analyze the as-built anchorage system. After discussion with Sandia National Laboratories' personnel, it was decided to terminate the analysis at a pressure of 74.123 psig. In the author's opinion, future work should be performed to obtain the pressure at which ductile or brittle failure occurs. This would validate the ASCE design equations for nuclear containment anchorage systems.

Cracks first occurred in the concrete surrounding the anchor plate as the anchor preload was applied. As internal pressure was applied, additional cracks formed in the vicinity of the anchorage system. Conical failure surfaces near the bottom ring and anchor plate started to form at 60 psig. All concrete surrounding the anchor bolt was cracked at 70 psig. At a pressure of 74.123 psig, a conical surface, with a slope of about 40 degrees from the horizontal, extended from the outer right edge of the bottom ring to the surface of the unfinished concrete.

The calculated strains in the knuckle, baseplate, anchor bolt, and the portion of the containment shell within the finite element model were well below the ultimate strain. The strain field in the shell was dominated by bending strain near the basemat/shell connection.

If the analysis had continued beyond 74.123 psig, enough cracks would probably have occurred to form a complete failure cone associated with the bottom ring. This would leave the anchor bolt as the only load transfer mechanism in the containment anchorage system. Hence, one could expect failure to occur in one of two possible modes: (1) formation of a complete failure cone above the anchor plate (brittle failure); or, (2) increase in the bolt strain with large deformation (ductile failure).

A finite element analysis of the containment anchorage system, which considers the parameters that affect this complex system, is feasible, but the convergence problems in ABAQUS have yet to be solved. A simple model, consisting of an anchor bolt embedded into a concrete block and subjected to a tensile load, should be studied. Solutions should be carried out for both brittle and ductile failures. Experimental calibration is strongly recommended to validate the finite element results.

1. INTRODUCTION

During the past few years, the integrity of nuclear containment buildings has become an important issue. Several researchers have increased efforts to investigate the performance of nuclear containment buildings during hypothetical severe accidents. Recently, the Containment Technology Division of Sandia National Laboratories (SNL) has developed methods for predicting the performance of light water reactor (LWR) steel containment buildings on behalf of the U.S. Nuclear Regulatory Commission. Most of these methods were validated using the results of scale model tests [1] and tests on penetrations, seals, and gaskets [2, 3, 4]. A failure criterion, based on the ultimate strain properties of the material and adjusted with knockdown factors, has been developed [5]. The failure criterion is applied to the results of finite element calculations to predict shell tearing and hence, leakage of steel containments.

A containment building fails to perform its function after a leak path is formed. Assuming that there are no pre-existing leak paths, a leak path can develop in a highly strained region of the containment, resulting in the leakage of radioactive material into the surroundings. The response of these regions under severe loading conditions and the conclusions from component studies are documented [6]. The objective of this investigation is to evaluate the performance of the Sequoyah nuclear containment building (see Figures 1.1 and 1.2) anchorage system under loading conditions beyond the design values.

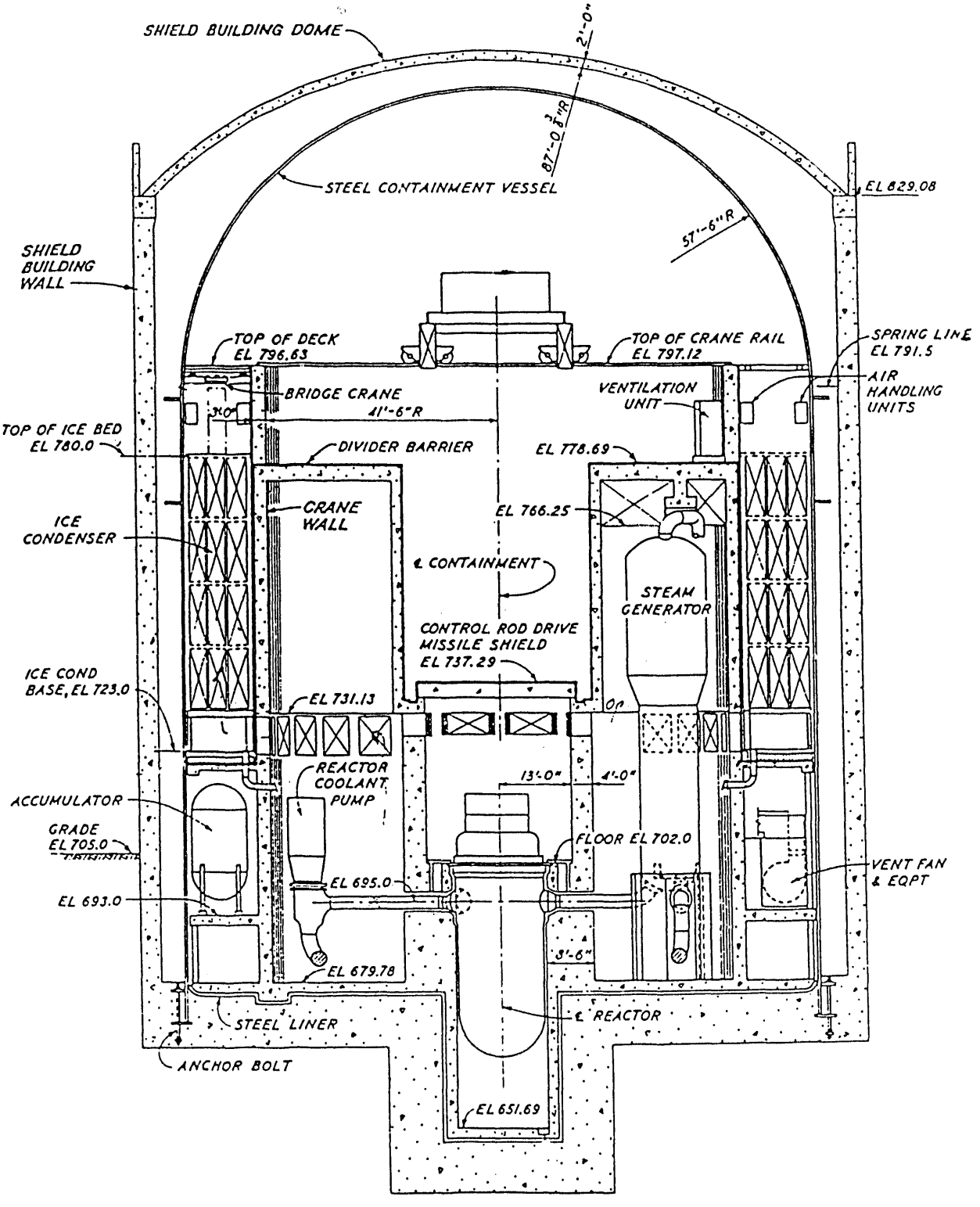

Figure 1.1 Sequoyah Containment Building

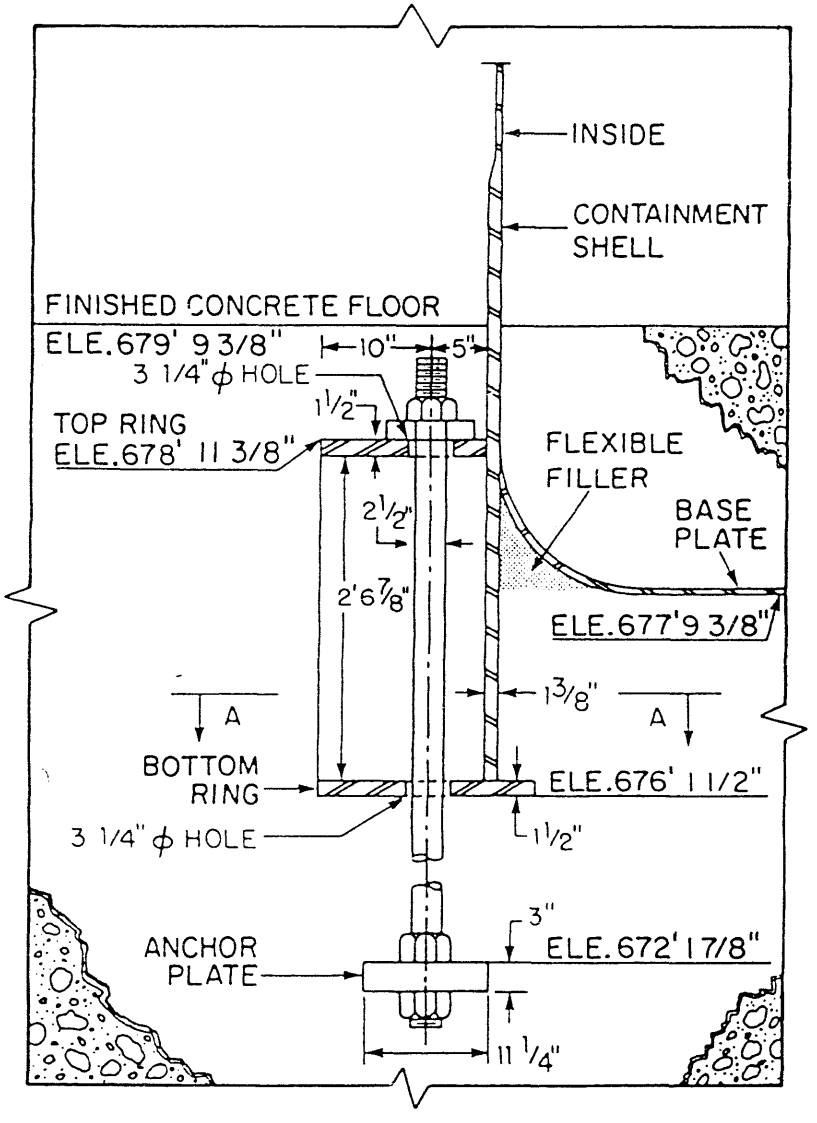

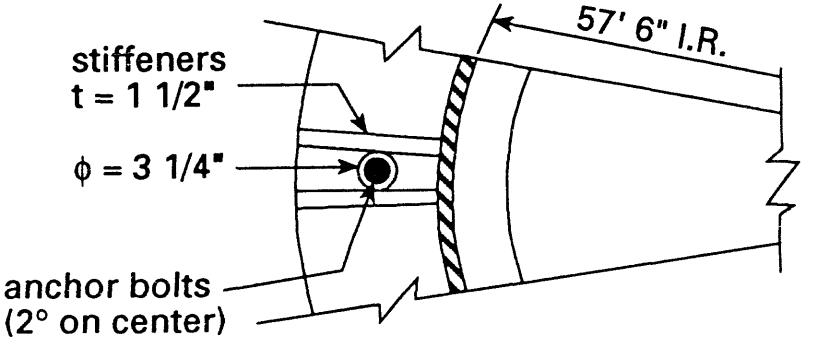

SEC A-A
NOT TO SCALE

Figure 1.2 Sequoyah Containment Anchorage System

2. ANCHORAGE FAILURE

Many steel containments in nuclear power plants are free standing structures held down by a number of high strength anchor bolts. These anchors are distributed around the containment building base and are embedded in a concrete floor (see Figure 1.2). Their function is to resist the uplift forces that are generated by internal pressurization of the containment or by seismic events. Failure of the anchorage system could introduce leak paths through the containment pressure boundary, and, thereby, compromise the containment integrity of the nuclear facility. Therefore, any evaluation of the performance of a containment under critical conditions must also examine the likelihood of this mode of failure.

In general, the failure modes of containment anchorage systems may be classified as (1) failure of the anchor bolt itself (ductile failure), and (2) failure in the concrete section (brittle failure). These two modes of failure are part of the basic performance criteria in concrete design. Brittle failure of a concrete connection is catastrophic, and thus, reinforced concrete structures are normally designed to ensure a ductile mode of failure. Ductile failure allows for movement and redistribution of forces. It provides some warning of impending collapse if the movement is being monitored.

Ductile failure results in the elongation of the bolts themselves. Typically, the bolts are made of ductile steel: for example, bolts with 16 percent elongation in a 2-inch gage length have been used in some containments. Therefore, it is reasonable to assume that the failure of these bolts occurs when the tensile stress exceeds the bolt material tensile strength, F_u. The containment pressure, P_{ub}, at which bolt failure would occur may be estimated as simply,

$$P_{ub} = \frac{n A_b F_u}{\pi r^2} \tag{1}$$

where n is the number of bolts (180 bolts), A_b is the bolt cross-sectional area (5.23 in^2), and r is the radius of the containment vessel (57′ 6"). Equation 1 yields a failure pressure of 79 psig for the Sequoyah anchorage system [6]. This pressure was based on a tensile strength of 125 ksi for the anchor bolt.

Brittle failure occurs when the embedded steel anchor does not fail in tension but rather pulls out a section of the concrete, which is approximately conical. The failure is caused by diagonal shear forces and tension on the conical surface [7]. The containment pressure which causes brittle failure is calculated as:

$$P_{uc} = \frac{4 \sqrt{f_c'}\, A_n}{\pi r^2} \tag{2}$$

where f_c' is the concrete compressive strength and A_n is the total effective stress area for all anchor bolts, defined by the projected area of stress cones [7, 8]. The effective area, A_n, is limited by overlapping of the stress cones,

by intersection of the cones with the concrete surface, by the bearing area of the anchor heads, and by the overall thickness of concrete. With an assumed concrete compressive strength of 5000 psi, Reference [6] reported that the brittle failure mode will occur at a pressure of 135 psig.

Equation 2 does not account for additional strength provided by reinforcing steel crossing the surface of the failure cone. The shear area of the reinforcing steel that intersects the failure cone should be determined to obtain upper bound for shear strength based on dowel action of the rebars [9]. This was not used in predicting the pressure associated with the brittle failure listed in [6] since reinforcing steel was provided only at the bottom of the basemat as well as near the unfinished and the finished concrete levels [10]. However, these rebars were included in the finite element model described later in this report.

The procedure outlined above can be used to predict approximate pressures at which ductile or brittle failure may occur in an anchorage system of a nuclear containment. However, such a procedure does not account for the structural deformation of the anchorage system. In the event of a severe accident, the internal pressure may induce structural deformation of the anchorage system sufficient to result in the formation of leakage paths in the containment boundary. This structural deformation of the entire anchorage system is, in all likelihood, caused by a combination of the following: deformation of the anchor bolts, deformation of the stiffener assembly, concrete deformation, cracking of the containment base-mat, and containment shell deformation. In addition, large deformation of the knuckle plate and/or at the weld connecting this plate to the containment shell (see Figure 1.2) may result in another leakage path. Considering the complexity of this situation, a more comprehensive approach to investigate the behavior of the anchorage system is desirable. In this work the finite element method was chosen for the analysis of the Sequoyah containment anchorage system. The ABAQUS [11] finite element code was selected to accomplish this objective.

3. MODELING PARAMETERS

Analytical modeling using the finite element method requires consideration of all the parameters that influence the behavior of the structure. The complexities in concrete behavior stem from the nonhomogeneous nature of concrete, the combination and mutual interaction of microscopic properties of concrete and steel, destruction of bond in local areas and the tensile weakness of concrete with progressive cracking. These parameters must be evaluated in order to gain an insight into the sensitivity of the results to a specific parameter.

3.1 Bond in Concrete

The strength of reinforced concrete structures depends upon the bonding action at the interface between the reinforcing bars and the concrete. A realistic representation of bond behavior is, therefore, necessary for application in finite element analyses.

Special linkage elements, mainly springs, have been developed and used for representing bond behavior in finite element analyses of reinforced concrete structures. The stiffnesses of the springs in these linkage elements have been experimentally formulated from force-displacement data [12, 13]. Bond behavior has also been represented using a 'tension stiffening' concept, i.e., allowing the concrete to carry some tensile stress after cracking. Two methods exist to incorporate the tension stiffening effect: (1) by defining the post-cracking behavior of concrete through a tensile stress-strain relationship [14]; and, (2) by adjusting the stress-strain diagram of the tensile steel after the concrete has cracked [15]. The additional stress represents the total internal tensile force carried by the concrete between the cracks. It is lumped at the level of the tensile reinforcement and oriented in the direction of the rebars.

Appendix A summarizes the study conducted herein to investigate the most appropriate method to idealize the bond behavior in reinforced concrete for this finite element analysis. Since the tension stiffening approach has been known to stabilize the solution numerically, it was selected instead of bond-link elements for the purposes of this project [16]. Additionally, Method 1 (above) was chosen to incorporate the tension stiffening effect because ABAQUS has built-in provisions for this method. Details of the method used to model bonding are provided in Section A.1.

3.2 Shear Transfer

The transfer of shearing forces is of critical importance in reinforced concrete members. In finite element analyses, transfer of shearing forces through uncracked portion of concrete is controlled by the shear modulus G of the uncracked concrete. However, shear transfer through cracked concrete by aggregate interlocking and dowel action of main reinforcement introduces some difficulties.

Dowel action and aggregate interlocking were investigated by several researchers [17]. A comprehensive analytical expression to represent the dowel stiffness is still not available [18]. Most of the proposed analytical models for such stiffness are based on the concept of a beam on an elastic foundation and their applicability is limited to small dowel forces [18]. Dowel action and

aggregate interlocking have also been modeled by a reduced shear modulus G_1, in the material matrix. A constant reduced shear modulus was most commonly used. However, a shear modulus which decreases linearly with strain normal to the crack yields a better representation of shear behavior [19]. Reference [20] developed a hyperbolic expression to model shear transfer. The validity of the two approaches given in [19, 20] were investigated and the results are summarized in Appendix A. As described in Appendix A, the use of the linearly decreasing shear modulus was found to give satisfactory results and has, therefore, been selected for the current work.

4. ANALYSIS OF SEQUOYAH CONTAINMENT ANCHORAGE SYSTEM

4.1 Geometry of the Containment Building

The Sequoyah steel containment is a cylindrical steel structure fabricated with A516 Gr. 60 steel and is covered by a hemispherical dome (see Figure 1.1). At the bottom there is a 1/4-in. thick steel plate covered by two feet of concrete (see Figure 1.2). The transition between the cylindrical plates forming the containment wall and the base plate is made through a knuckle plate welded to both. The knuckle plate is formed from a 1/4 in. thick steel plate curved at an outer radius of 12 inches. The steel containment vessel is surrounded by a 3-foot-thick reinforced concrete shield building with an inside radius of 62.5 ft.

Anchorage for the steel containment vessel is provided by anchor plates (11.25 in. x 11.25 in. x 3 in.) at the lower end of high-strength preloaded anchor bolts. The anchorage system is designed in such a way that uplift forces are transferred from the steel vessel through top and bottom rings to the top of the bolts, (see Figure 1.2). These rings are strengthened by 1 in. thick vertical stiffeners located on each side of each anchor bolt. The bolts are 2.5 inches in diameter and are distributed circumferentially around the base of the containment vessel at 2 degree intervals. The bolts are preloaded to 25 ksi and embedded in a 12-foot-thick concrete mat. The basemat is anchored into the rock foundation with several tie rods grouted into 10- to 15-foot deep holes.

4.2 Finite Element Model

The symmetrical arrangement of the anchor bolts around the base of the containment vessel makes it possible to select a one-degree wedge extending from the center of one bolt to midway to the next bolt (see Figure 1). The model includes portions of the containment vessel, shield building, anchor bolt, anchor plate, vertical stiffener, reinforced concrete mat, and soil foundation material (see Figure 4.1).

From the theory of plates and shells, bending is a local phenomenon whose effect diminishes at a distance of approximately $3\sqrt{rt}$, where r and t are the mean radius and the thickness of the cylindrical structure [21]. With this consideration, the heights of the shield and containment buildings in the model were 500 in. and 92 in., respectively. The authors recognize that the shield building has little or no effect on the structural behavior of the containment anchorage system. However, it was necessary to include a portion of the shield building in the model to account for the effects of its dead weight on the pressure distribution beneath the basemat.

The finite element mesh was developed using Release 2.2 of PATRAN [22]. Figure 4.1 illustrates an outline of the finite element mesh used in the analysis. Eight-node solid elements (C3D8 in ABAQUS) were used to model the containment basemat and the shield building. The size of the solid elements within the failure cone associated with the brittle failure mode explained in Section 2 was reduced. Reinforcing steel where provided in the basemat were modeled utilizing the rebar option in the ABAQUS program. The containment shell, bottom plate, knuckle plate, top and bottom rings as well as the vertical stiffener were modeled using 4-node shell elements (S4R5 in ABAQUS). The anchor bolt was idealized using beam elements (B31 in ABAQUS).

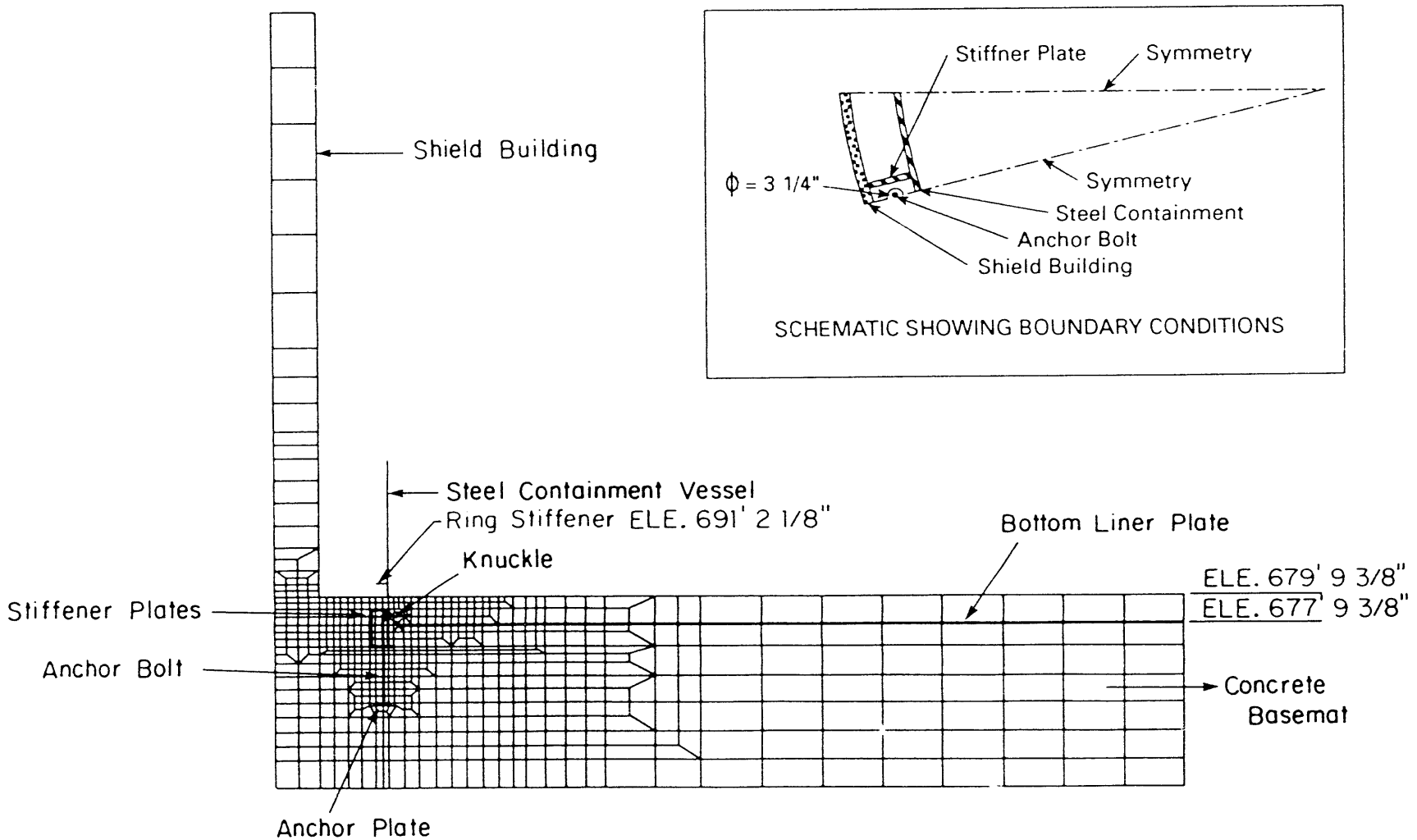

Figure 4.1 Finite Element Model of the Sequoyah Containment Anchorage System

The concrete-rock interface at the bottom of the basemat was idealized by compression-only springs (Spring1 in ABAQUS) whose stiffness was calculated by multiplying the foundation subgrade modulus times the tributary area for the spring. At locations where there were tie rods between the rock and the concrete mat, concrete-rock interface was idealized by nonlinear tension-compression springs (Spring1 in ABAQUS). All interfaces between the steel plates, containment shell, bottom liner plate and concrete elements were modeled using compression-only springs (Spring2 in ABAQUS). These springs were orientated perpendicular to the steel with stiffness calculated as those beneath the basemat. Frictional forces were neglected at the interface. Appropriate boundary conditions were imposed on the symmetry planes of the model (see Figure 4.1). The model has 1935 elements and 4000 nodes.

4.3 Material Model

4.3.1 ABAQUS Concrete Model

The concrete model in ABAQUS is mainly for plain concrete [11]. However, a reinforced concrete element can be modeled by combining the plain concrete model with rebar elements. These rebar elements are superimposed on the mesh of plain concrete elements and are used with standard metal plasticity models that describe the behavior of the rebar material. Cracking in the concrete model in ABAQUS is assumed to occur when the stresses reach a failure surface. The concrete model in ABAQUS is a smeared crack model in the sense that it does not track individual macro cracks. Smeared crack models are known to produce finite element results that are "mesh sensitive" [11]; however, mesh sensitivity was not considered in the work reported herein. The ABAQUS theoretical manual [11] documents that tension stiffening (Section 3.1) in conjunction with smeared cracking is a practical solution to the cracking problem.

4.3.2 Concrete Properties

The concrete constitutive model in ABAQUS requires input of several parameters, including points from the stress versus plastic strain curve in uniaxial compression, concrete uniaxial tensile strength, concrete biaxial compressive strength, principal component of plastic strain at ultimate in biaxial compression and principal stress at cracking in plane stress when the other nonzero principal stress component is at its ultimate compressive stress value.

Points used to define a piecewise linear relationship for the uniaxial compressive stress and plastic strain were calculated using Hognestad stress-strain relationship in [23]. The stress-plastic strain relationship for concrete under uniaxial compression is shown in Figure 4.2. The values for the remaining material parameters are listed in Table 4.1. ABAQUS default values were used for those parameters requiring biaxial test data since this information was not available. Bond and shear transfer in cracked concrete were accounted for as discussed in Appendix A, and Sections 3.1 and 3.2.

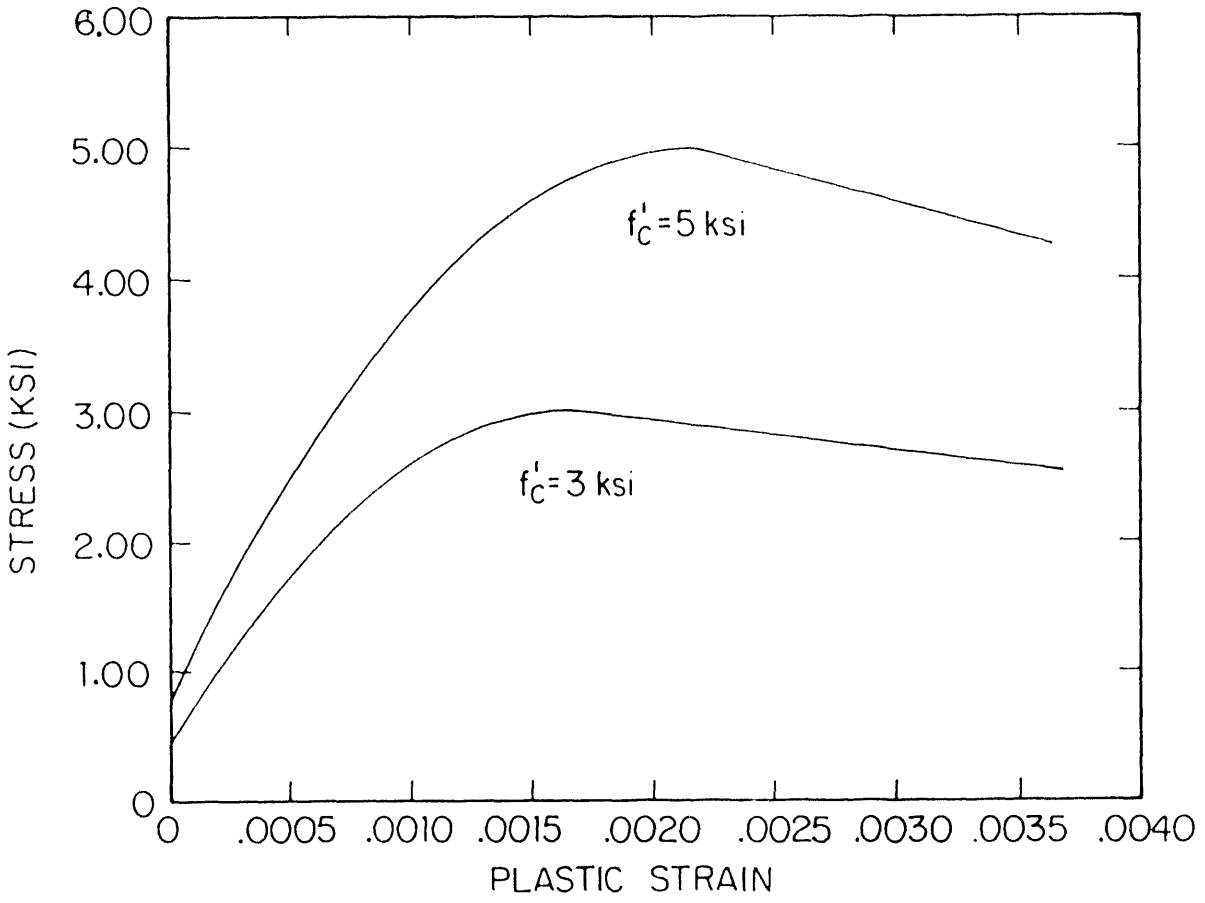

Figure 4.2 Stress-Plastic Strain Data for Concrete Under Uniaxial Compression

Table 4.1 Additional Material Parameters Used With the Concrete Constitutive Model in the ABAQUS Code

Parameter Description	Value
Young's Modulus	57,000 $\sqrt{f_c'}$ psi
Poisson's Ratio	0.167
Ratio of the biaxial ultimate compressive stress to the uniaxial compressive ultimate stress	1.16*
Absolute value of the ratio of uniaxial tensile stress at failure to uniaxial compressive stress at failure	0.09*
Ratio of principal plastic strain at ultimate stress in biaxial compression to the plastic strain at ultimate stress in uniaxial compression	1.28*
Ratio of the tensile principal stress at cracking in plane stress when the other nonzero principal stress component is at the ultimate compressive stress to the ultimate cracking stress under uniaxial tension	1/3*

* Default value in ABAQUS Code

4.3.3 Steel Properties

The true stress-strain curve for A516 Gr. 60 for the different thicknesses was obtained from engineering stress-strain data [24]. The stress-plastic strain relationships for the different plate thicknesses are shown in Figure 4.3.

4.4 Loading and Solution Strategy

In the first step of the analysis, the dead weight of the containment basemat and the anchor pre-load were applied. The dead load of the finite element model was represented utilizing body forces of 150 lb/ft^3. Bolt pre-load was simulated by cooling the anchor bolt gradually until a stress of 25 ksi was induced in the bolt. In the second step, the weight of portions of the steel containment and the shield building not within the finite element model were applied. To account for the weight of components within the containment building (see Figure 1.1), a pressure of 500 psf was assumed to act on the basemat. In addition, the weight of the concrete walls inside the containment was applied as a pressure acting on the elements beneath the walls.

Following the application of the dead load and prestress load, an internal pressure was applied. Pressures were applied on both the containment shell and basemat. Meridional forces associated with the applied internal pressure were calculated and were applied upward at the top nodes of the containment shell (see Figure 4.1). This pressure was increased from zero to 30 psig in three steps. The load step size was then decreased to 5 psig up to a pressure of 40 psig. Beyond this pressure and up to a pressure of 70 psig a load step size of 2 psig was used. This was further reduced to 1 psig and the analysis was carried to 73 psig. However, a singularity problem was encountered when the pressure was increased from 73 to 74 psig. The load step size was then decreased to 0.2 psig and the analysis was successfully performed to 73.8 psig. Once again, a singularity occurred between 73.8 and 74 psig. The solution was restated from 73.8 psig using a pressure increment of 0.01 psig.

Convergence in ABAQUS is attained when the maximum residual nodal forces are less than a user-specified tolerance, which is defined as small fractions of the applied nodal forces. A convergence tolerance of 1.5 kips was used up to a pressure of 40 psig. Following this pressure, the tolerance value was relaxed to 2.5 kips. A sufficient number of iterations were allowed during each load step until a converged solution was reached. The convergence criterion was met in each increment of the analysis. The effect of the residual force tolerance on the structural response cannot be quantified unless the structure is analyzed using different tolerances. However, the results after each load step showed that the displacements increment from one iteration to the next were very small. The largest residual force which occurred during the analysis was about 2.2 percent of the total applied nodal forces. This was associated with a vertical degree of freedom.

No converged solution was obtained when the pressure was increased to 74.13 psig. At this pressure numerical problems were encountered during the analysis. The ABAQUS program indicated that the "plasticity algorithm did not converge at some nodes." However, the program did not identify the location of these nodes. The load step size was decreased to 0.001 psig and the analysis was continued. Converged solutions were reached as the pressure was increased

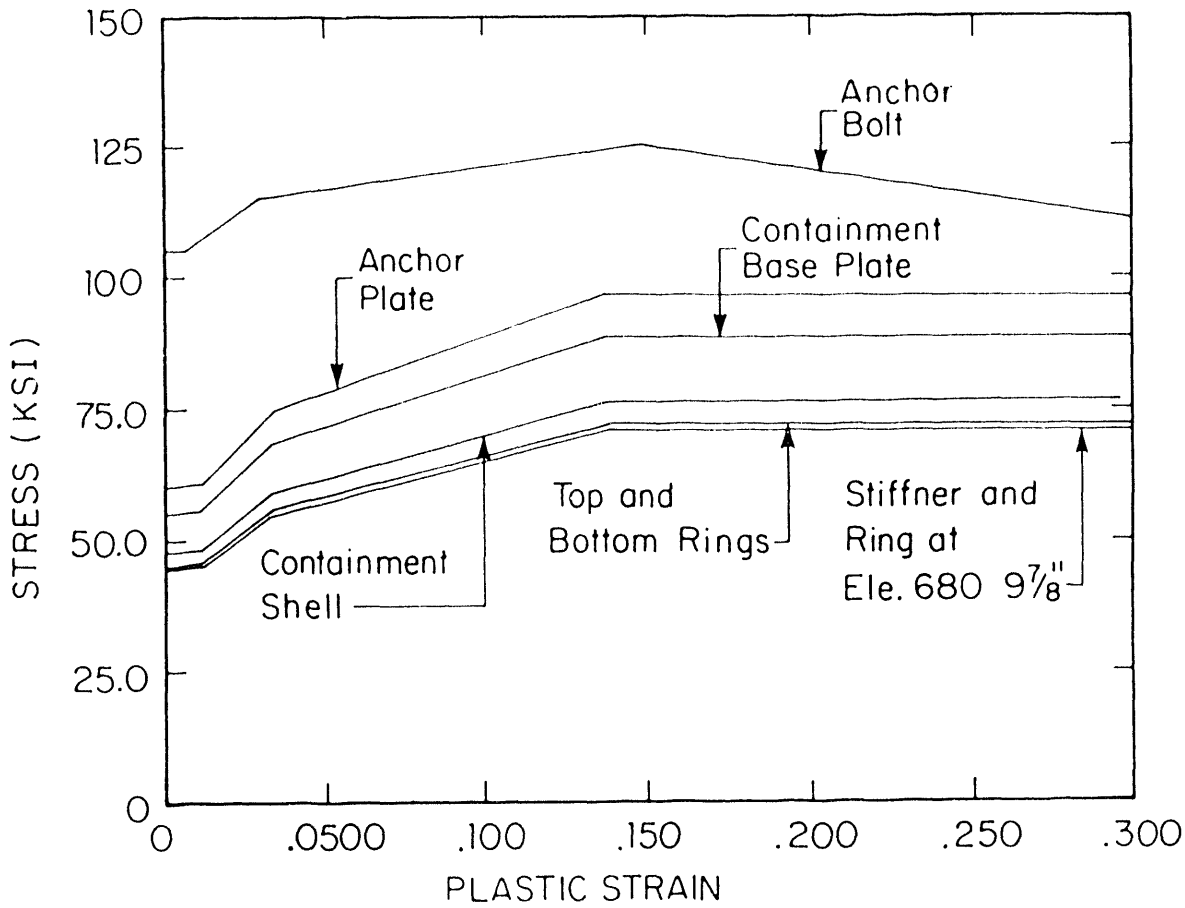

Figure 4.3 True Stress-Plastic Strain Relationships for the Steel Components Included in the Finite Element Model

to 74.123 psig; however, the plasticity convergence problem was again encountered beyond this pressure. ABAQUS personnel were consulted regarding this nonconvergence problem [25, 26]. They suggested using a smaller model with a few elements to analyze the containment anchorage system. In such a model the anchor bolt and the anchor plate were to be approximated by axisymmetric elements. This type of model was not pursued since the objective of this work is to investigate the as-built anchorage system. After discussion with Sandia personnel [27], it was decided to terminate the analysis at this pressure. Future work should be performed to determine the pressure at which ductile or brittle failure of the containment anchorage system occurs.

4.5 Results

4.5.1 Concrete Cracking

The cracking sequence along the symmetry plane through the anchor bolt in the basemat is illustrated in Figures 4.4 through 4.10. The ABAQUS output file lists the direction cosines of the normals to the three principal planes. In these figures the element is shown as cracked if a crack exists at, at least, one integration point (eight integration points/element). When cracks were formed at more than one integration point, crack orientation was determined by averaging the crack slopes. Cracks were initiated in the first principal direction (referred to as Crack 1 in the ABAQUS output file) in the concrete surrounding the anchor plate as the anchor bolt pre-load was applied. These cracks are shown as heavy lines in the figures. As the pressure was increased to 20 psig, additional cracks were formed in the concrete below the bottom ring (see Figures 4.4 and 4.5). These cracks propagated down toward the anchor plate as additional pressure was applied (see Figures 4.6 through 4.10). Cracks were also formed above the bottom ring at a pressure of 50 psig (see Figure 4.7). Additional cracks were initiated in the concrete above the anchor plate. At 60 psig, more cracks were formed. Conical failure surfaces appeared to be developing at the anchor plate and the bottom ring (see Figure 4.8 and discussion in Section 2). When the internal pressure was increased to 70 psig (see Figure 4.9), all concrete elements between the anchor plate and the bottom ring as well as the elements just below the anchor plate were cracked. The cracks below the anchor plate were horizontal, while the cracks forming the conical surfaces on the left and right of the top ring and anchor plate range between 30 and 40 degrees from the horizontal (see Figure 4.9). When the pressure was increased to 74.123 psig, a conical surface with a slope of 40 degrees from the horizontal was formed on the right of the bottom ring. This surface extended from the bottom ring to the surface of the unfinished concrete beneath the 1/4 in. steel plate (see Figure 4.10).

The analysis also predicted that cracks were formed in the other principal directions. Cracks in the second principal direction (defined as Crack 2 in ABAQUS output) were initiated at a pressure of 30 psig in the region below the bottom ring (see Figure 4.5). These cracks are illustrated in Figures 4.5 through 4.10 as dashed lines. The cracks in the second principal direction were propagated in the radial direction and down toward the anchor plate as the pressure was increased above 30 psig. When the applied internal pressure

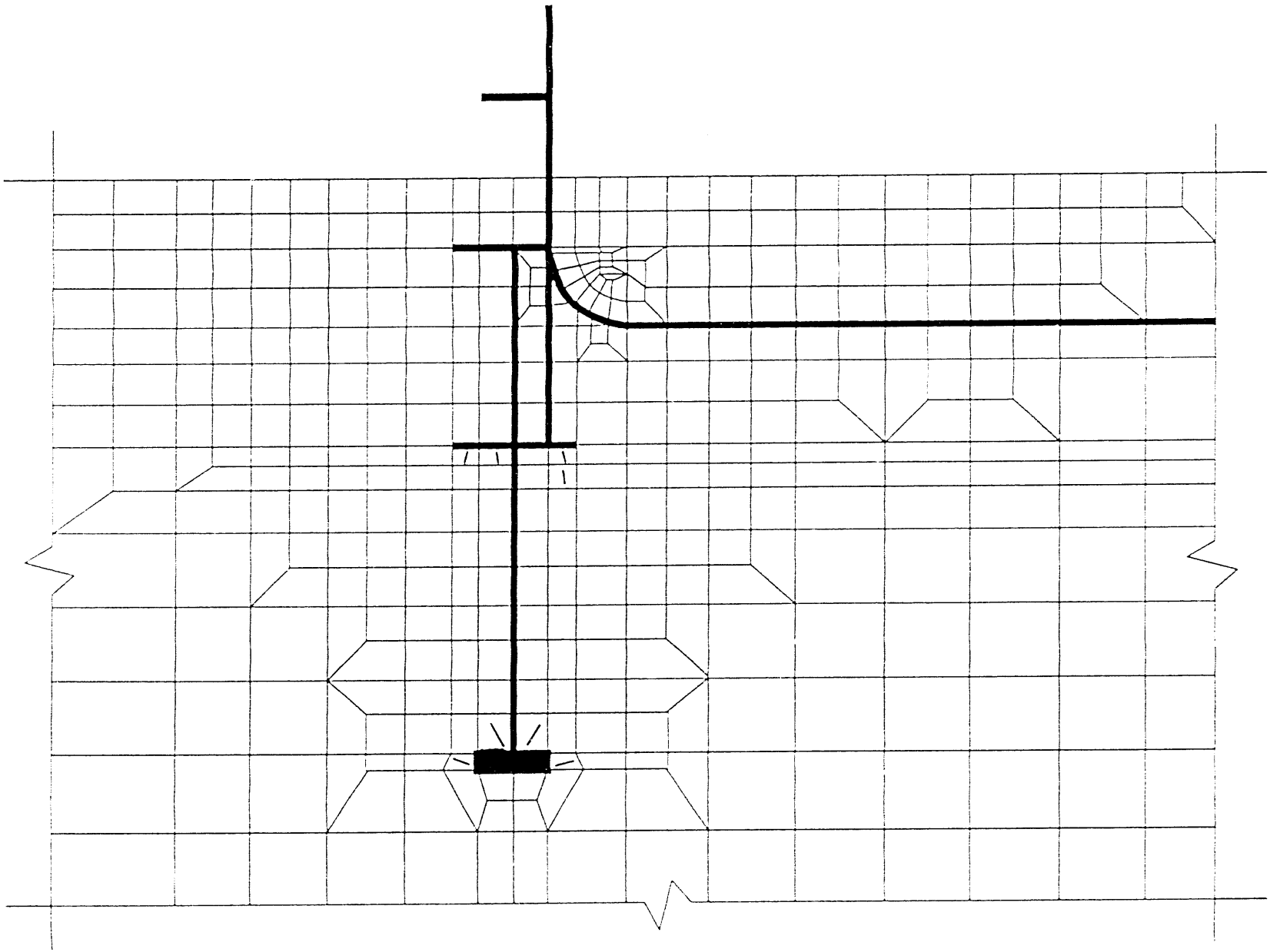

Figure 4.4 Development of Cracks in the Containment Basemat at 20 psig

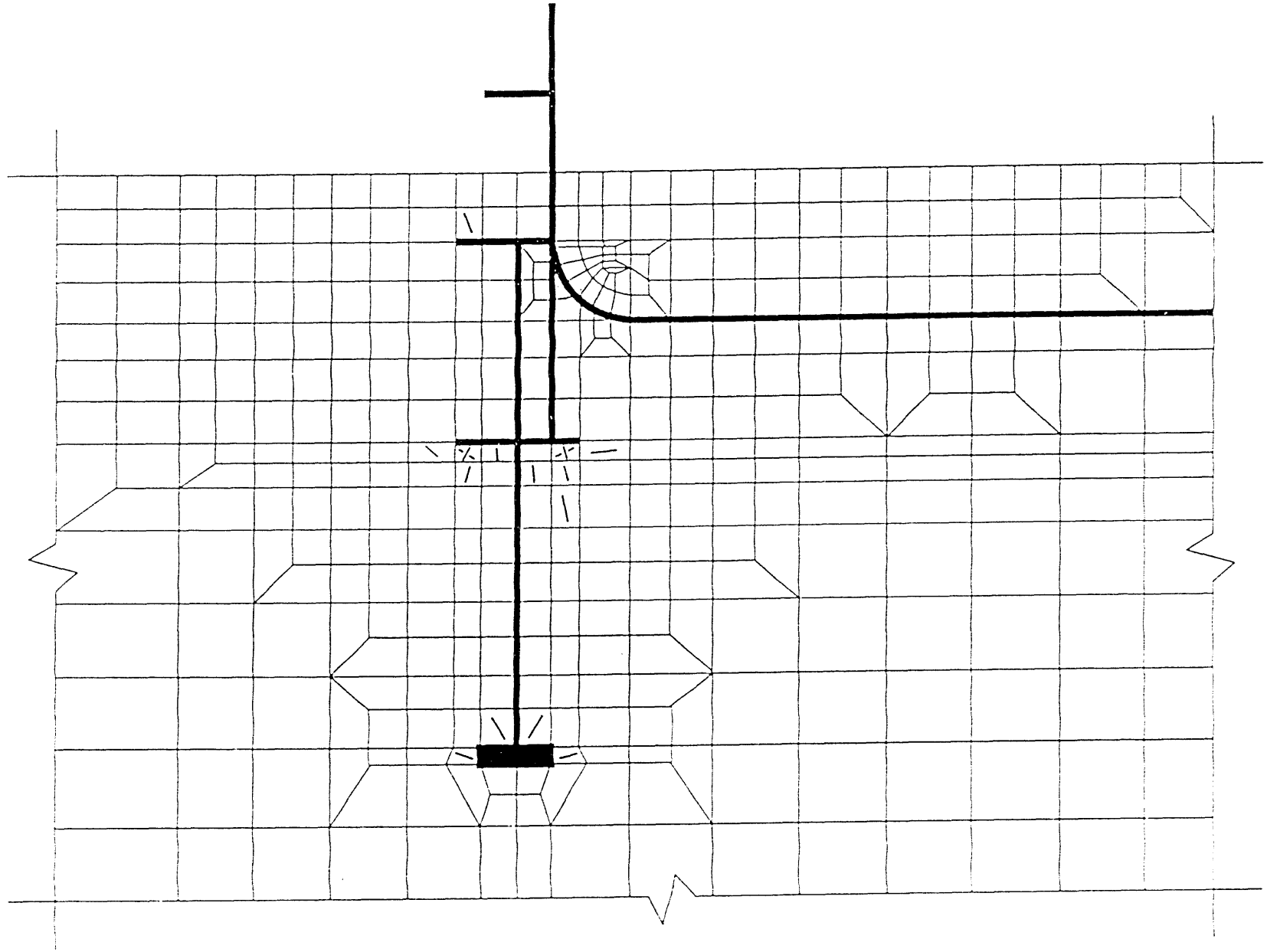

Figure 4.5 Development of Cracks in the Containment Basemat at 30 psig

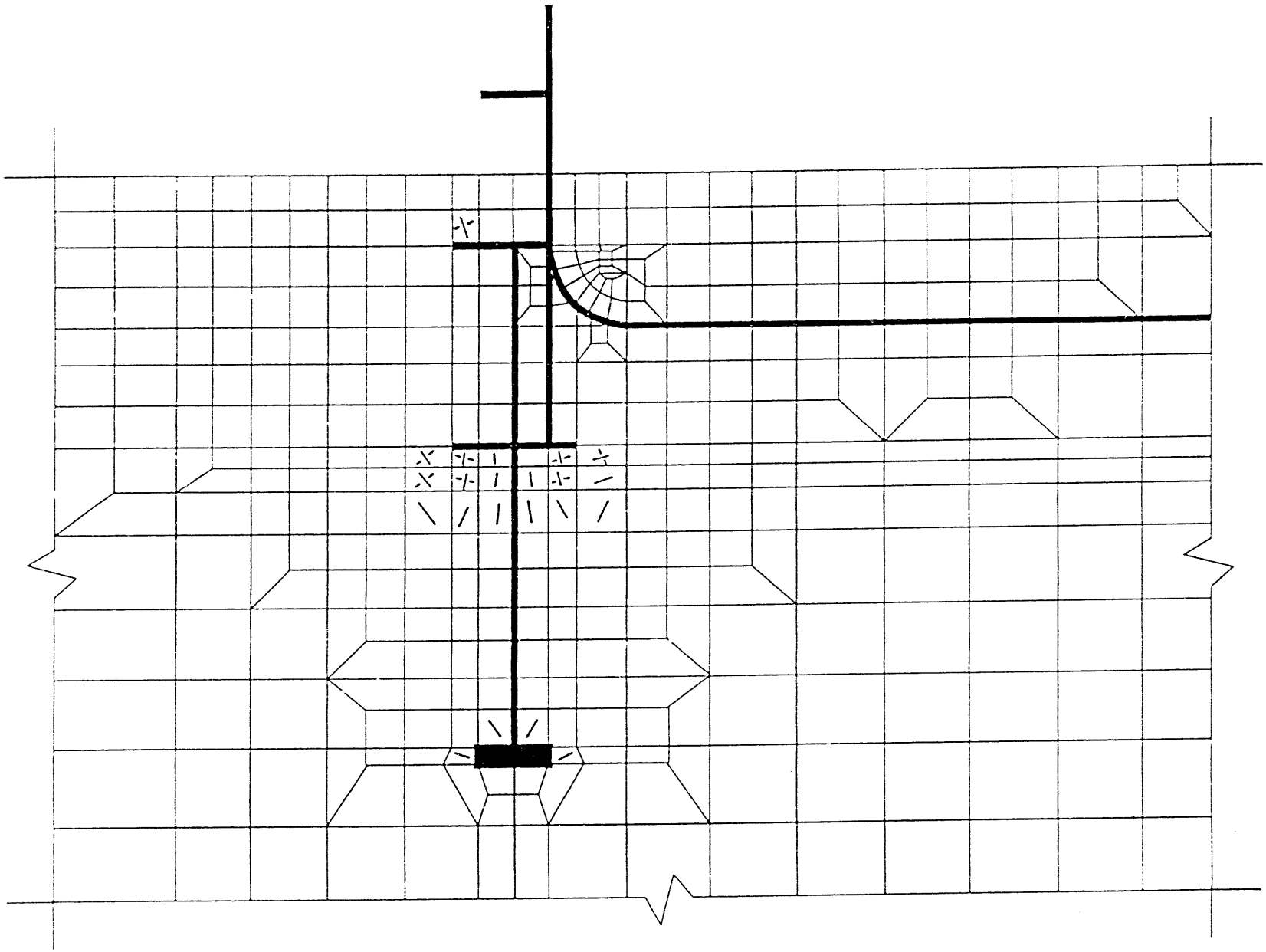

Figure 4.6 Development of Cracks in the Containment Basemat at 40 psig

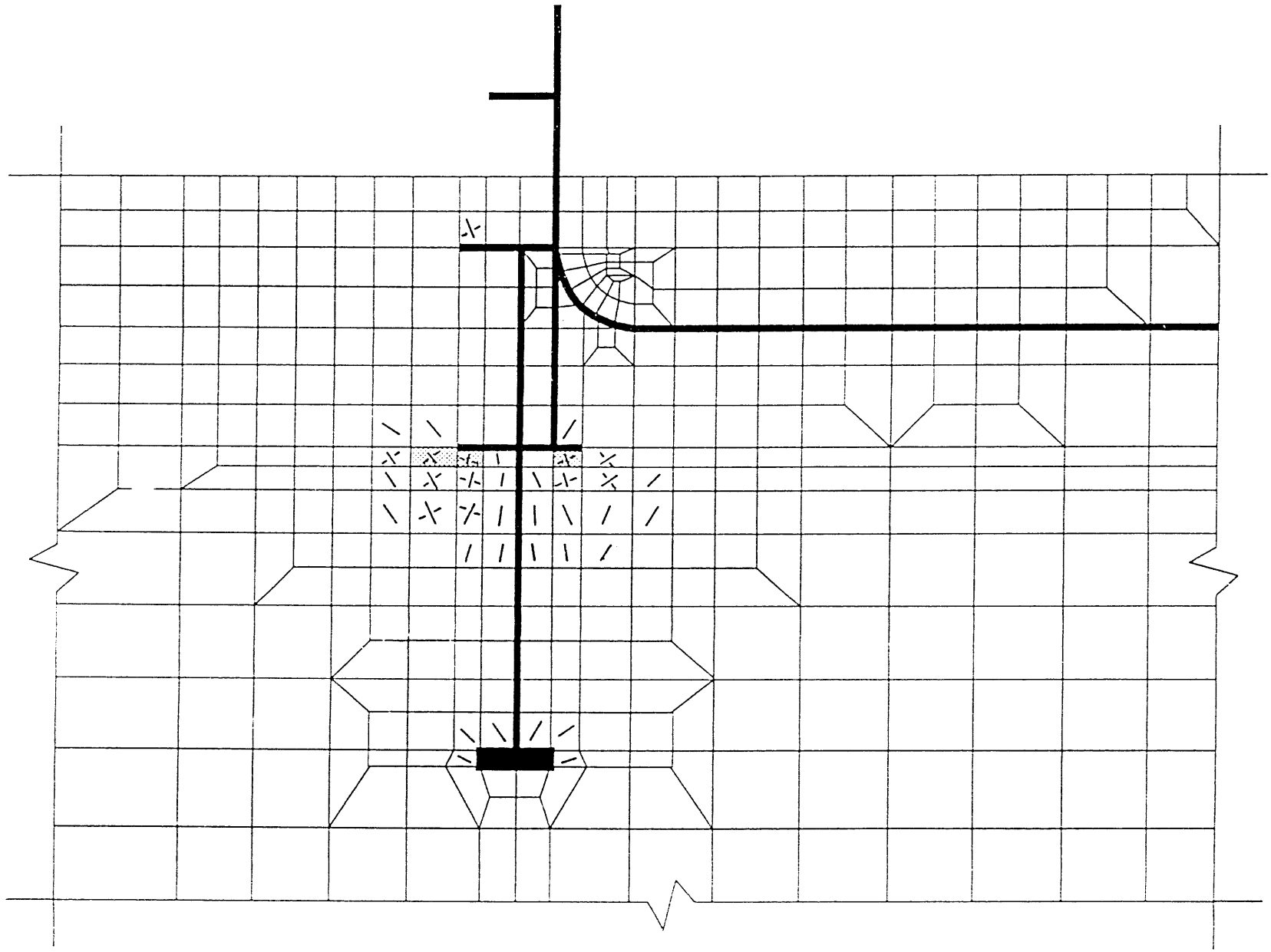

Figure 4.7 Development of Cracks in the Containment Basemat at 50 psig

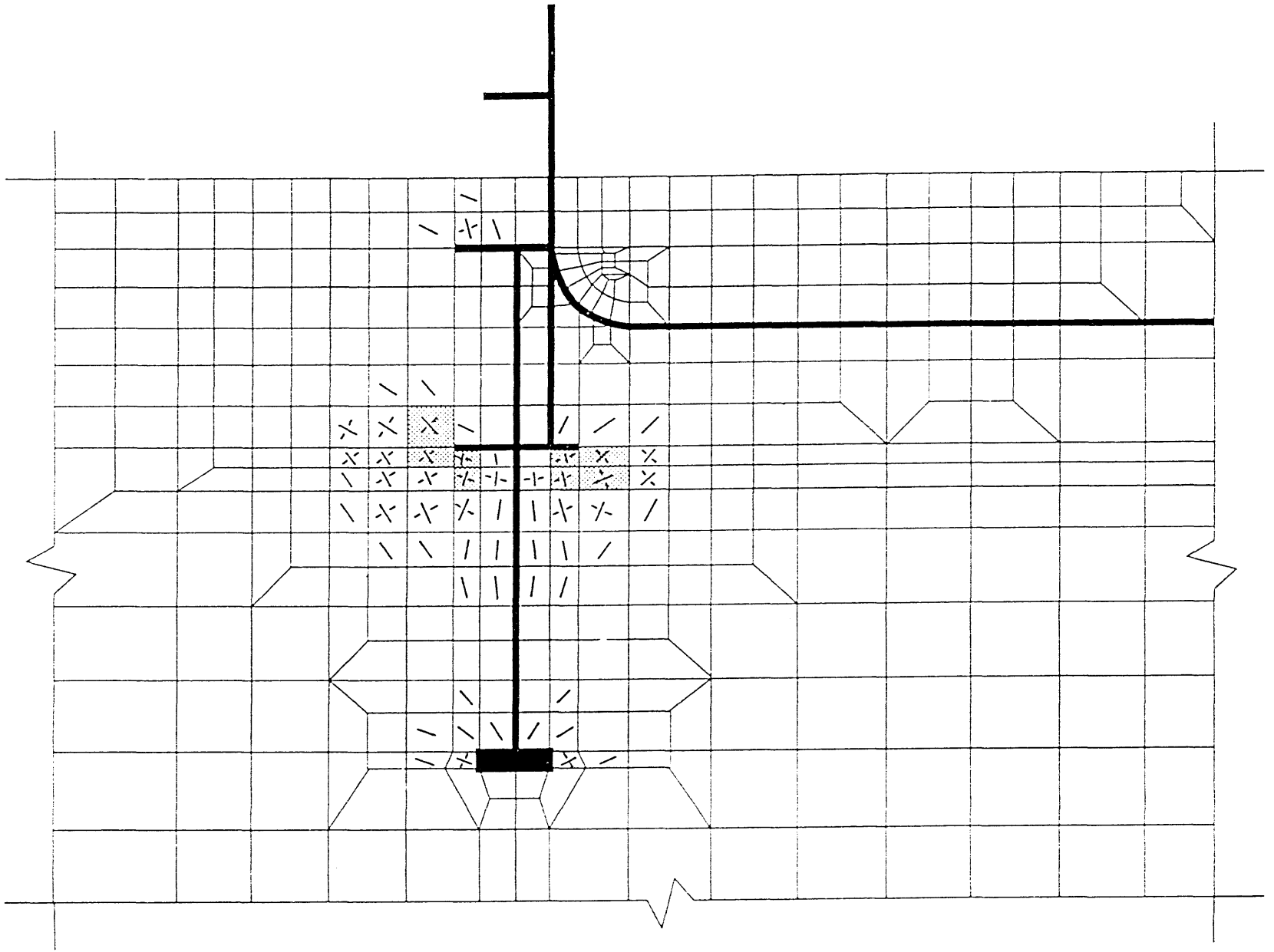

Figure 4.8 Development of Cracks in the Containment Basemat at 60 psig

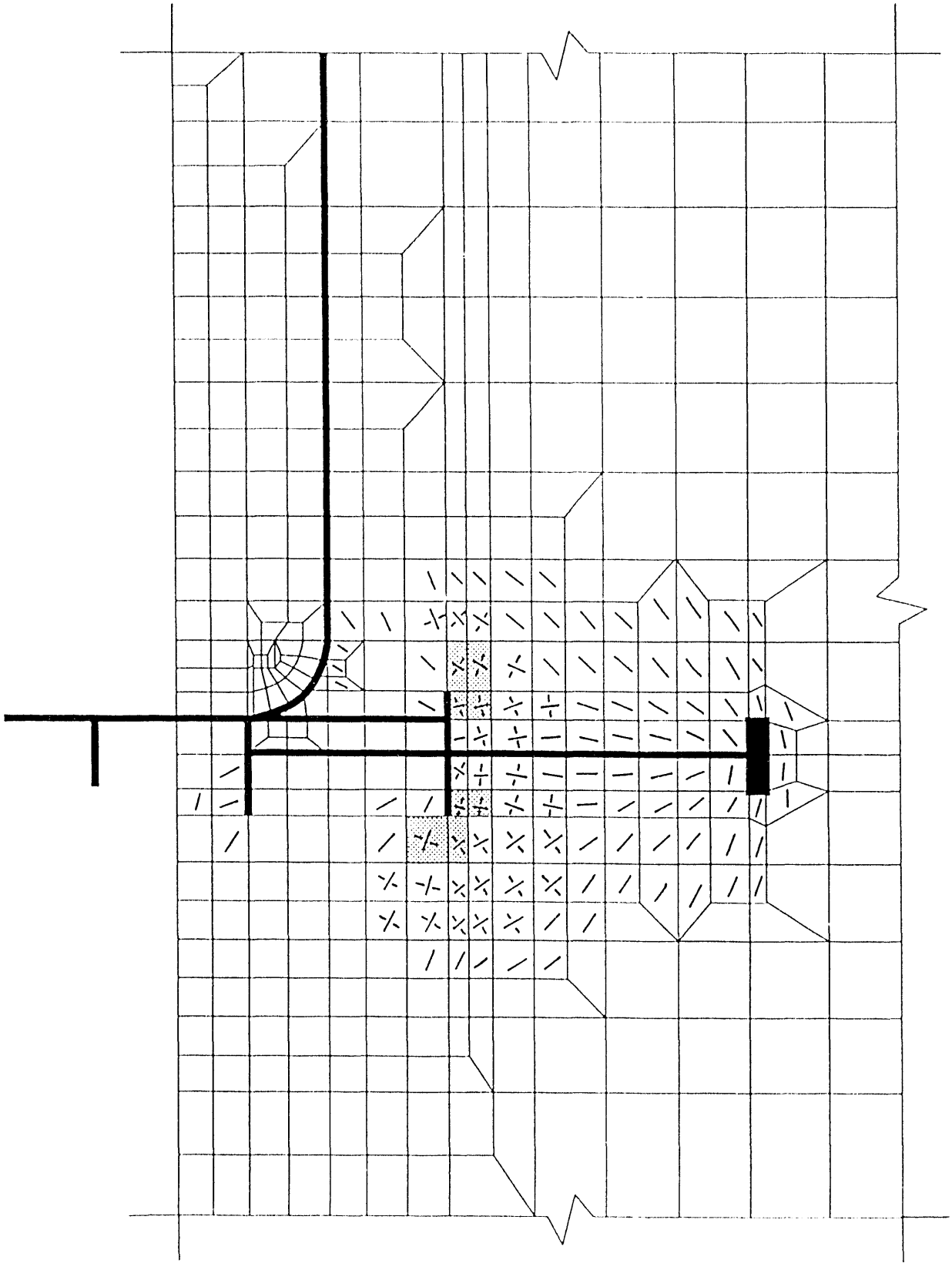

Figure 4.9 Development of Cracks in the Containment Basemat at 70 psig

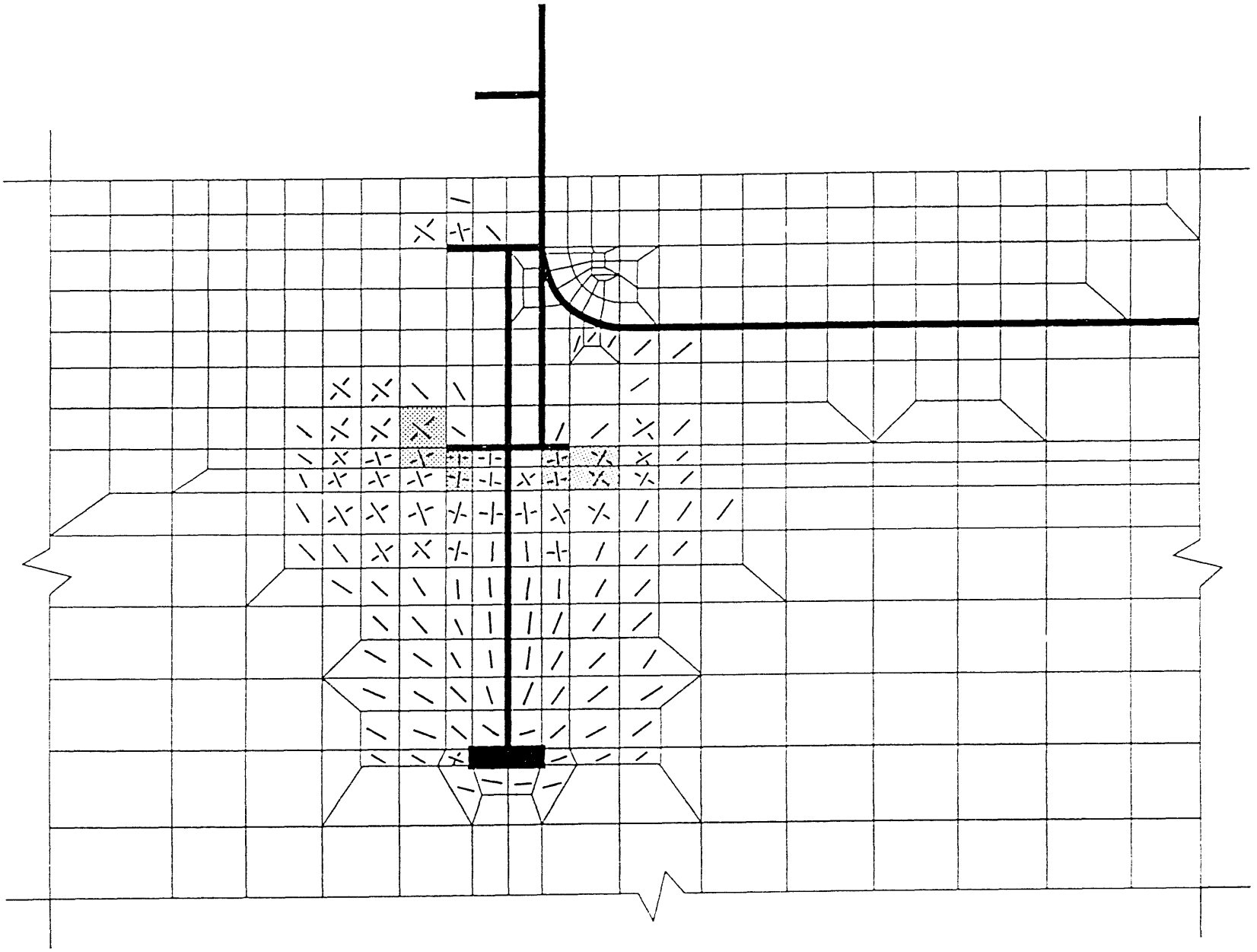

Figure 4.10 Development of Cracks in the Containment Basemat at 74.123 psig

reached 50 psig, cracks started to form in the third principal direction (referred to as Crack 3 in ABAQUS output file) in the concrete just below the left and right of the bottom ring. (Note that cracks in the third principal direction are parallel to the symmetry plane, that is, parallel to the view in Figures 4.4 to 4.10. Elements that are cracked in all the three principal directions are shaded in Figures 4.5 through 4.10.)

Cracks were also initiated in the concrete above and to the left of the top ring at a pressure of 30 psig (see Figure 4.5). The analysis indicated that inclined cracks began to form in the concrete to the left of the top ring as the pressure reached 60 psig (see Figure 4.8). No additional cracks were detected in this area as the pressure was increased to 74.123 psig.

4.5.2 Deformed Shape

A sequence of deformed shapes for the concrete elements in the basemat in the vicinity of the anchor bolt is shown in Figures 4.11 to 4.13. At low pressures these deformed shapes illustrate that the concrete cover above the top and bottom rings behave as short-deep cantilevers subjected to an upward forces (see Figure 4.12). As the internal pressure increases, the moments, M_1 and M_2, shown in Figure 4.14 also increase. The resulting tensile stresses in the radial direction cause cracking on the left of these two rings (see cracks in Figures 4.4 through 4.10). (Note: All moments shown in Figure 4.10 are those acting over the entire section.)

Similar behavior was also present at low pressures in the regions below the bottom ring. Notice the discontinuity in the basemat caused by the embedded portion of the containment shell. In other words, one can view the discontinuity as a built-in crack in the basemat (see Figure 4.15). Vertical cracks beneath the bottom ring were initiated by the tensile stresses in the radial direction induced by the moment M_3 (see Figure 4.14). This moment was caused by the weight of the shield building and the upward pressure beneath the basemat. This moment increases since the soil pressure beneath the basemat decreases as the containment internal pressure increases. The increasing M_3 propagated additional cracks beneath the bottom ring, toward the anchor plate.

4.5.3 Component Loads

Prior to pressurization of the containment, the preload of the anchor bolt was transferred to the basemat through the anchor plate and the top ring. As the applied internal pressure was increased from 10 to 20 psig, the applied upward forces were balanced by the bolt's preload. Additional applied pressure was then transferred to the basemat through the top and bottom rings pressing against the concrete above these rings. Portions of the applied load were also transferred to the base plate and to the anchor plate. Figure 4.16 shows the portions of the load carried by the top ring, bottom ring, anchor bolt and the knuckle plate. The figure indicates that beyond a pressure of 40 psig, most of the load was transferred to the basemat through the bottom ring. Notice that the rate of the increase of the anchor bolt force is small. However, this rate increased beyond a pressure higher than 40 psig. This occurred after the cracking of the concrete above the top and bottom ring were progressed. At higher pressures it is anticipated that larger portions of the load will be

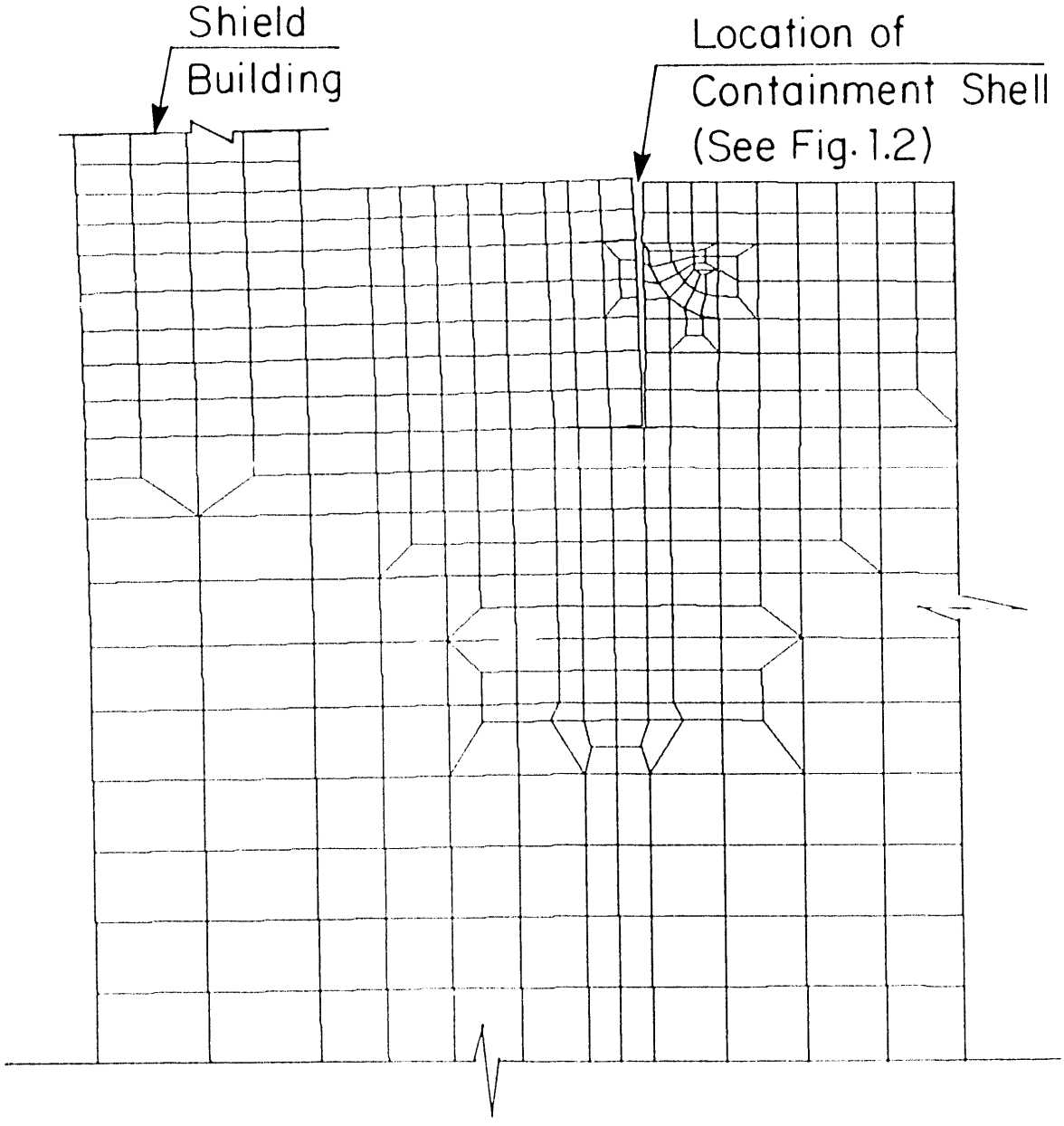

Figure 4.11 Deformed Shape for the Sequoyah Containment Basemat in the Vicinity of the Anchorage System at 20 psig - No Cracks are Shown (Magnification Factor = 200)

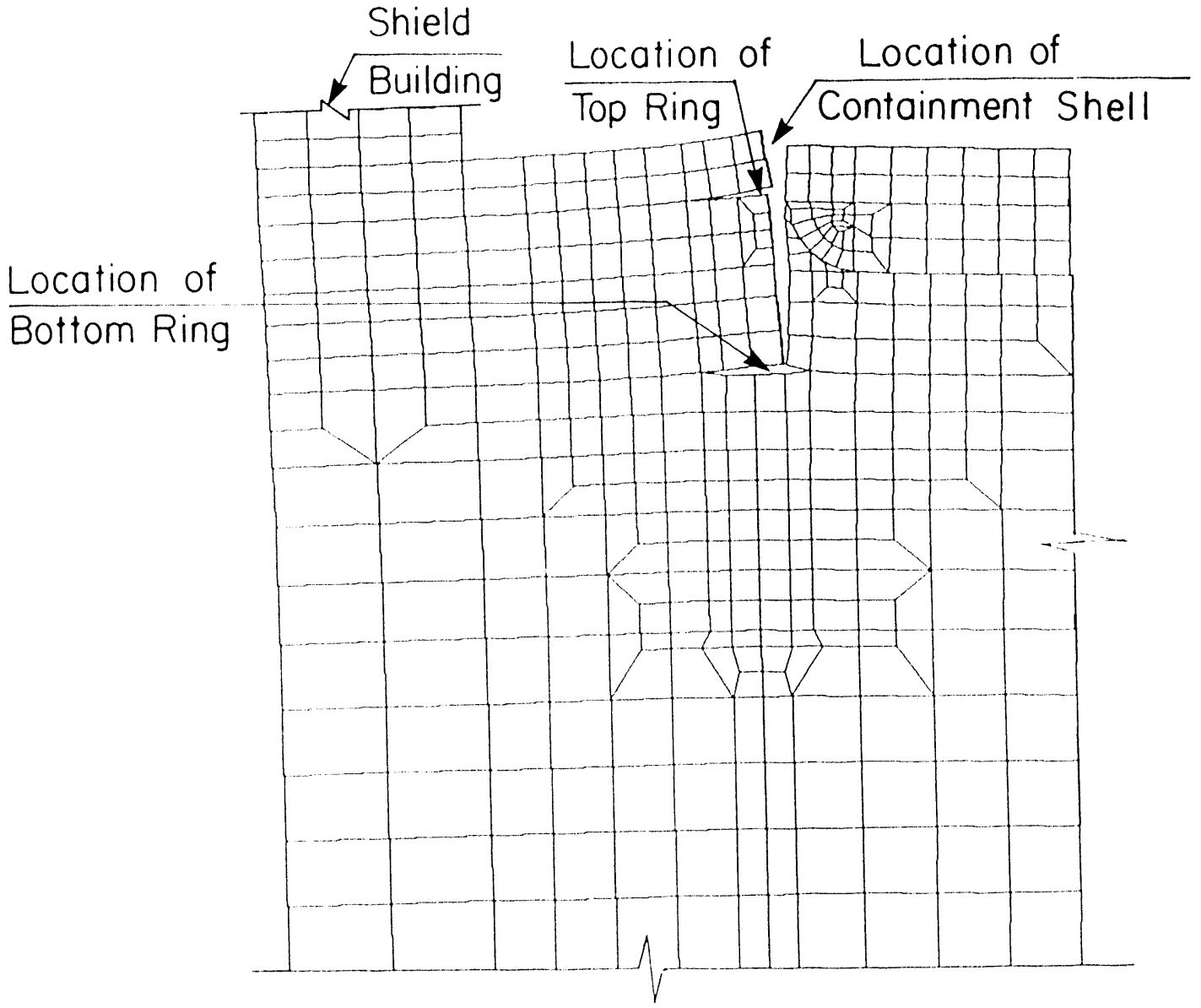

Figure 4.12 Deformed Shape for the Sequoyah Containment Basemat in the Vicinity of the Anchorage System at 50 psig - No Cracks are Shown (Magnification Factor = 200)

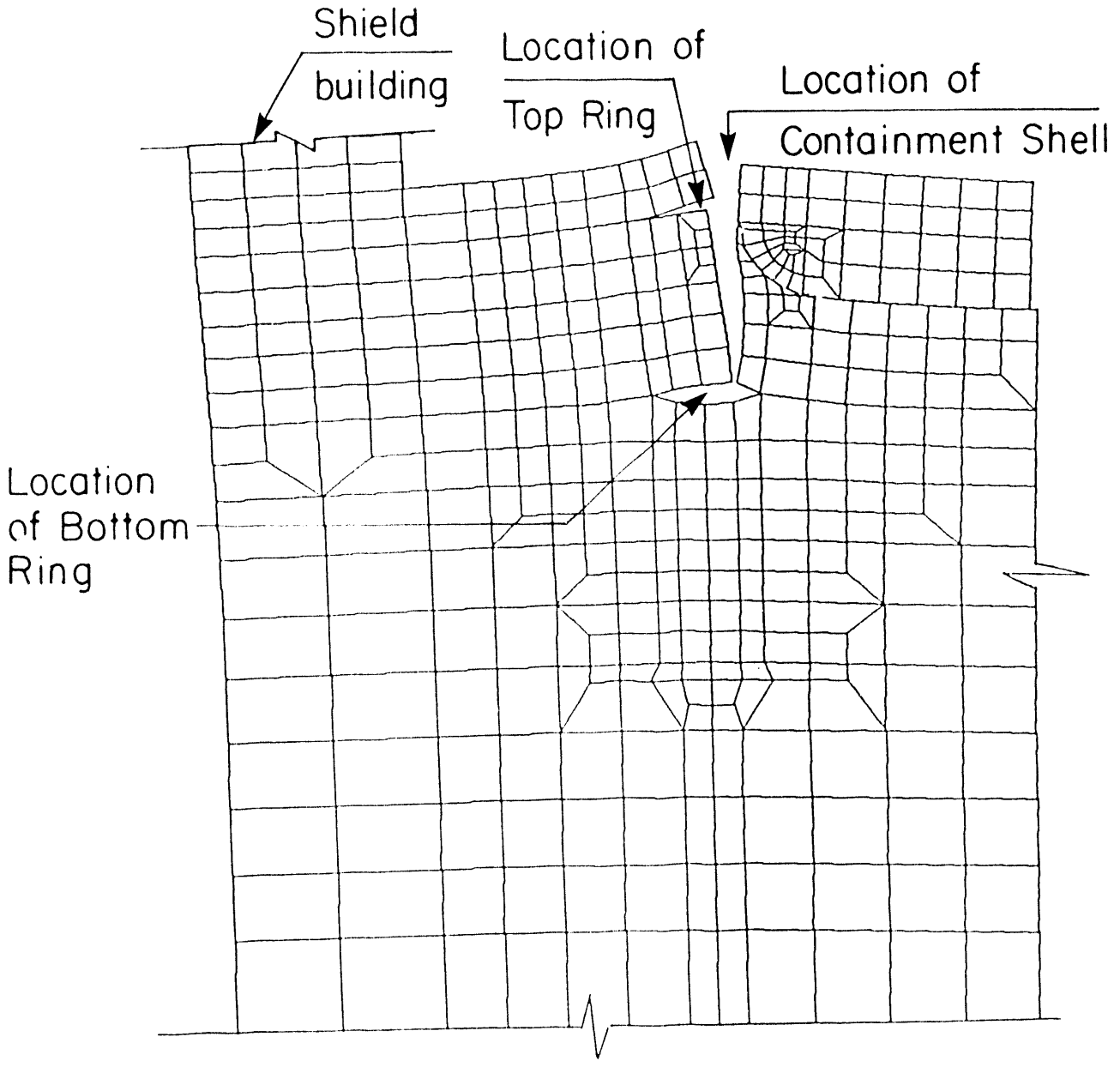

Figure 4.13 Deformed Shape for the Sequoyah Containment Basemat in the Vicinity of the Anchorage System at 74.123 psig - No Cracks are Shown (Magnification Factor = 200)

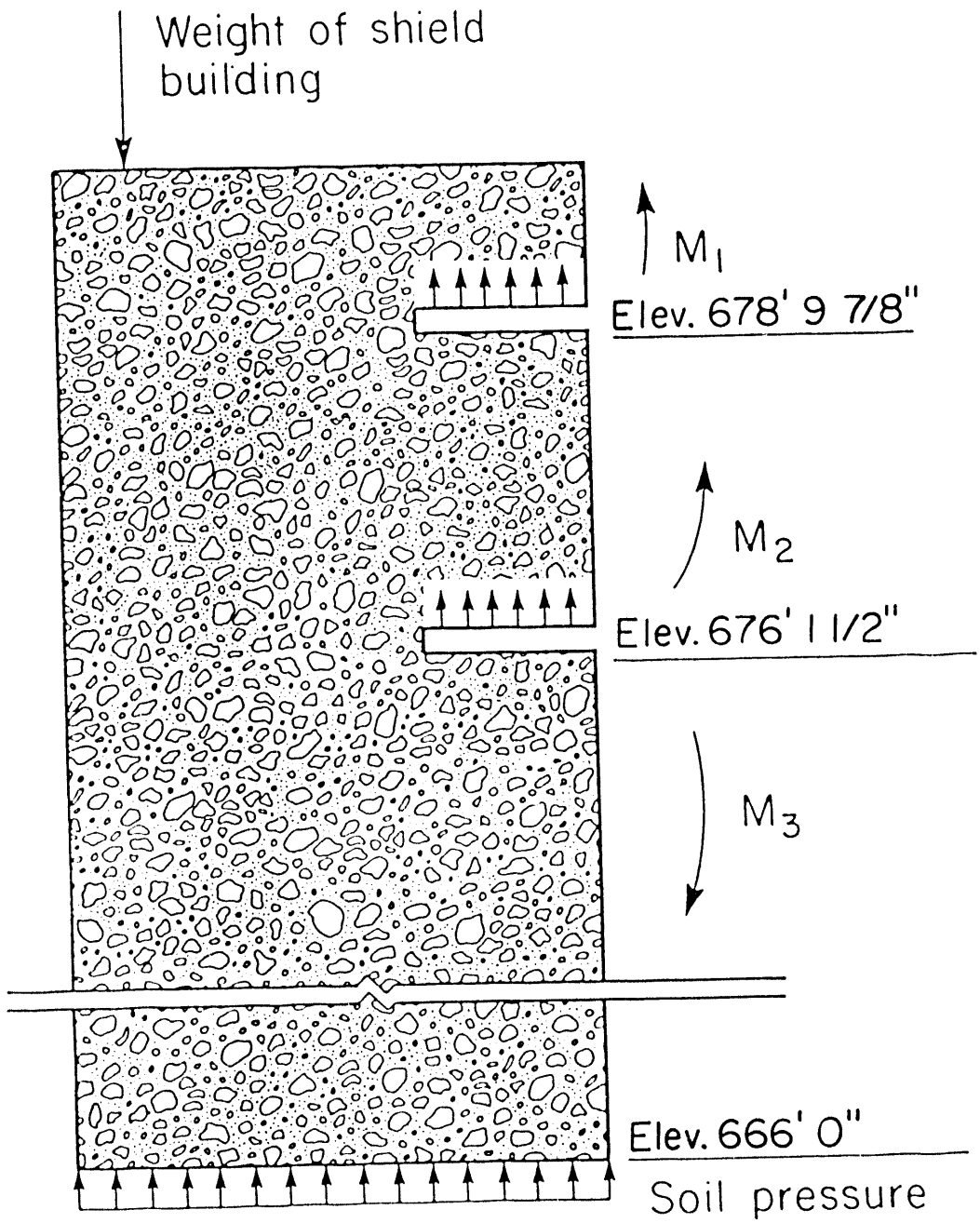

Figure 4.14 Loads Acting on Containment Basemat in the Vicinity of the Anchorage System (Anchor Bolt not Shown)

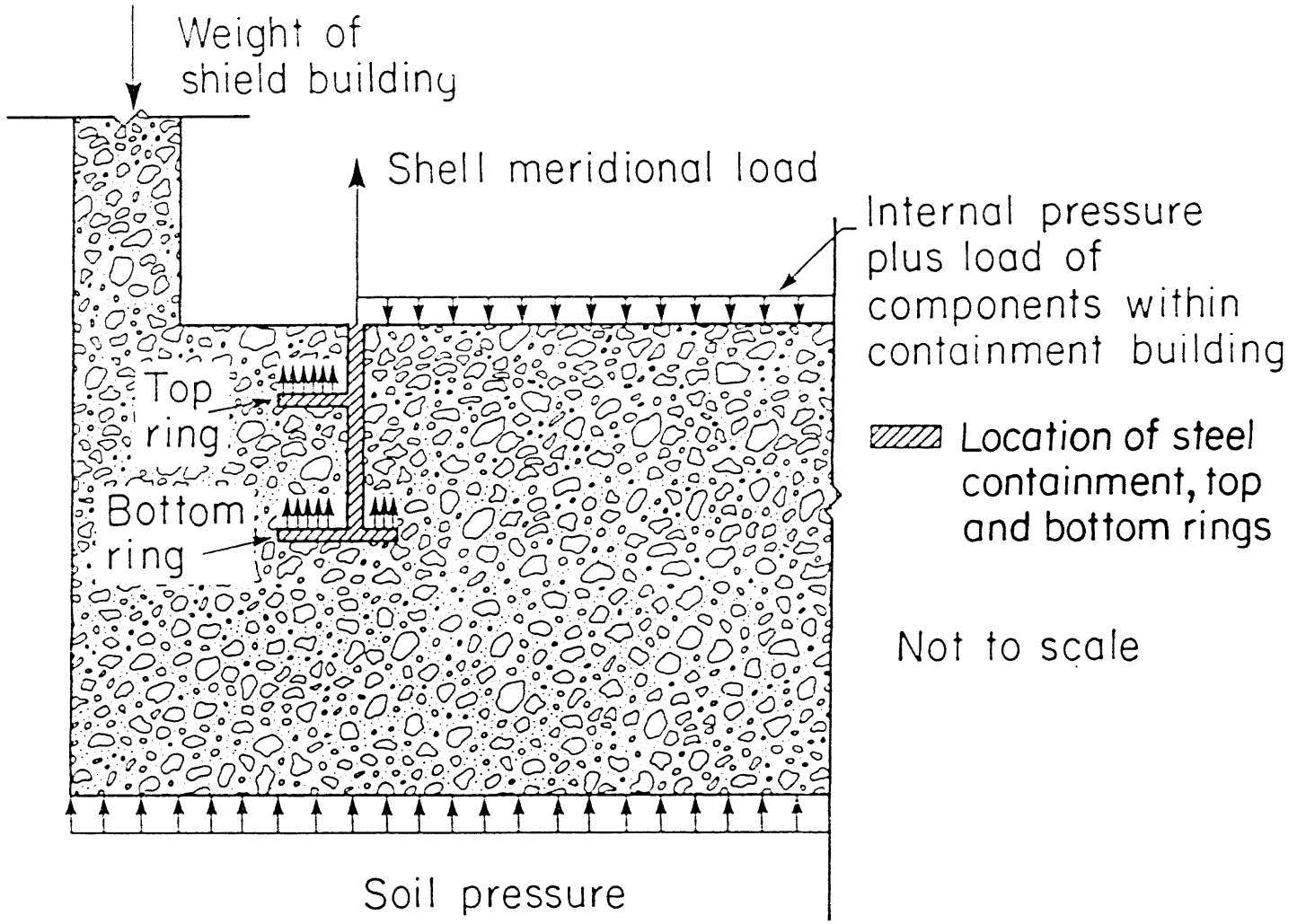

Figure 4.15 Schematic Showing the Built-in Crack in Containment Basemat Near the Containment Anchorage System

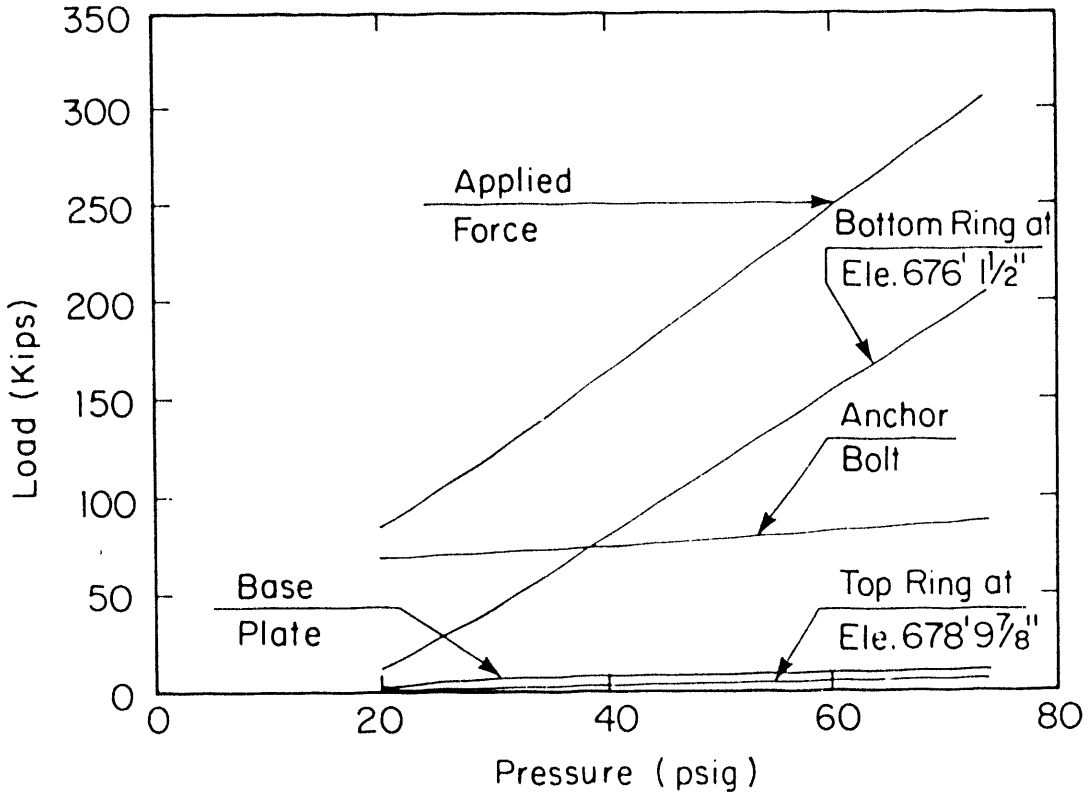

Figure 4.16 Fraction of Total Meridional Shell Load Carried by Each Component in the Containment Anchorage System

carried by the anchor bolt as more cracks develop in the vicinity of the anchorage system. When complete failure cones associated with both the top and bottom rings are formed, the anchor bolt will carry the entire applied load.

Figure 4.16 indicates that the force transferred to the knuckle plate and the top ring were insignificant. The fraction of the load carried by the knuckle plate remained almost constant (about 2%) throughout the loading process. At a pressure of 74.123 psig, the force transferred to the knuckle plate was approximately 512 lb/in. This resulted in a stress of 1925 psi in the 3/8 in. fillet weld between the knuckle plate and the containment shell.

4.5.4 Steel Strains

Figure 4.17 shows the stresses in the anchor bolt as a function of the applied pressure. Notice that the axial stress in the bolt is not zero at zero applied pressure, but equal to the prestress of 25 ksi. The stress in the anchor bolt increases with internal pressure. The rate of the increase in the bolt stress increases with the applied pressure because more cracks were formed in the containment basemat and more load is transferred to the anchor bolt.

The axial strain in the anchor bolt at 74.123 psig is 0.1% which is well below the anchor bolt material's ultimate strain. Hence, a ductile failure in the anchor bolt is unlikely prior to the development of a complete failure cone associated with the bottom ring Elev. 676' 1 1/2" (see Figure 1.2).

The maximum surface strain in the portion of the containment shell that was included in the model is illustrated in Figure 4.18. At 74.123 psig, the maximum meridional strain was 0.192 percent on the inside surface of the shell near Elev. 679' 9 3/8". This strain was comprised of a membrane and bending strains of 0.056 and 0.136 percent, respectively. Thus, the strain field was dominated by bending strain caused by the bending of the shell near the shell/basemat connection. The finite element results also showed that there was insignificant bending strains near the top of the modeled portion of the containment building. This illustrated the adequacy of the assumption of including only a portion of the containment up to a height equal to $3\sqrt{rt}$, where r and t are the containment radius and thickness respectively (see Section 4.2). The circumferential surface strain is also shown. The maximum circumferential strain at 74.123 psig was 0.135 percent. These strains are well below the failure strain predicted in [5] in which the complete containment shell was analyzed. Reference [5] reported a peak strain of 10.7% in the steel containment near the spring line at a pressure of 81 psig.

The maximum surface strain in the knuckle is shown in Figure 4.19. The strain in the 1/4" knuckle plate at 74.123 psig is 0.084 percent. This strain was comprised of membrane and bending strains of 0.013 and 0.071, respectively. Notice that the strain in the knuckle plate is not zero at zero pressure. This is caused by the anchor preload.

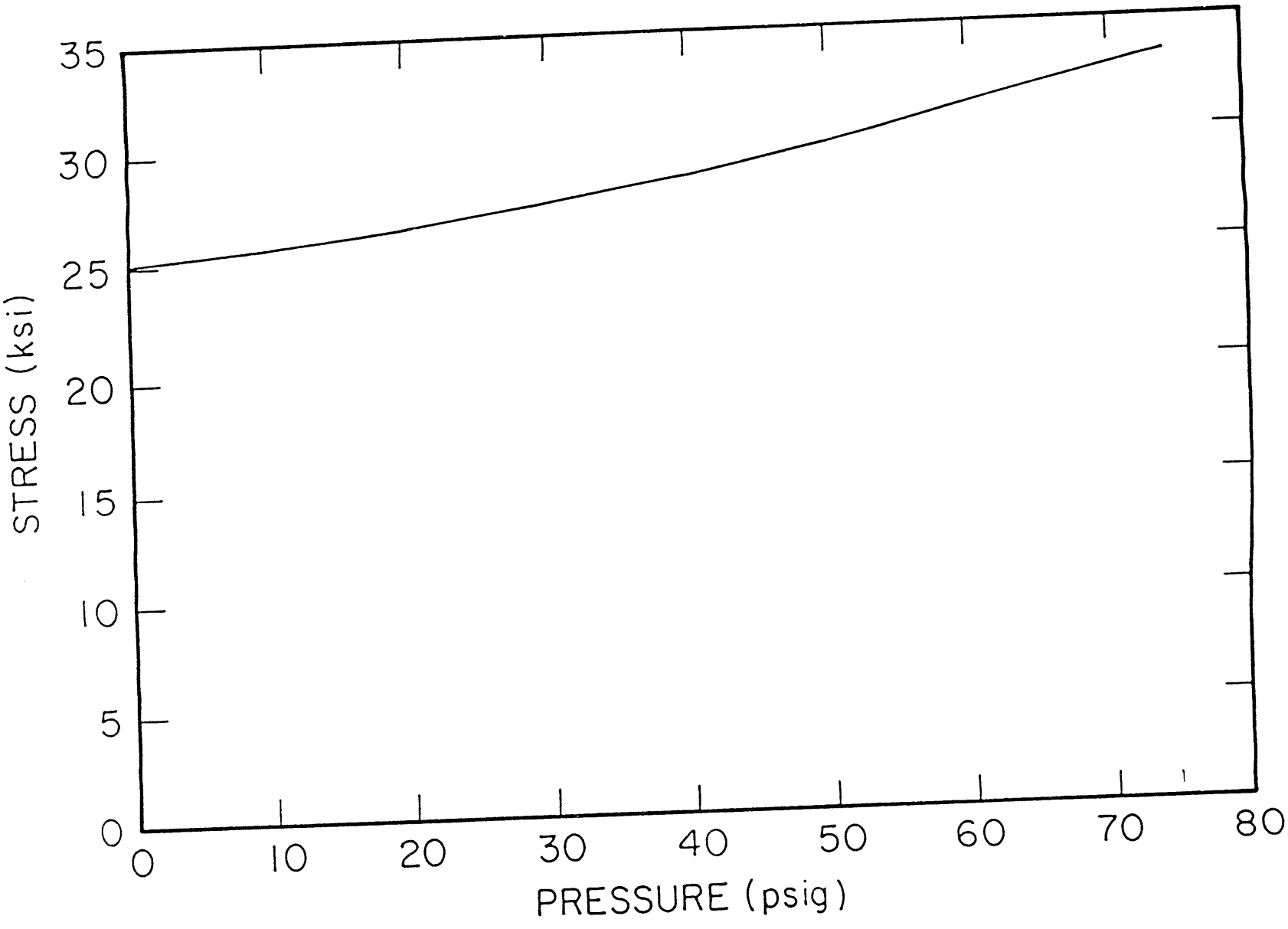

Figure 4.17 Anchor Bolt Stress-internal Pressure Relationship

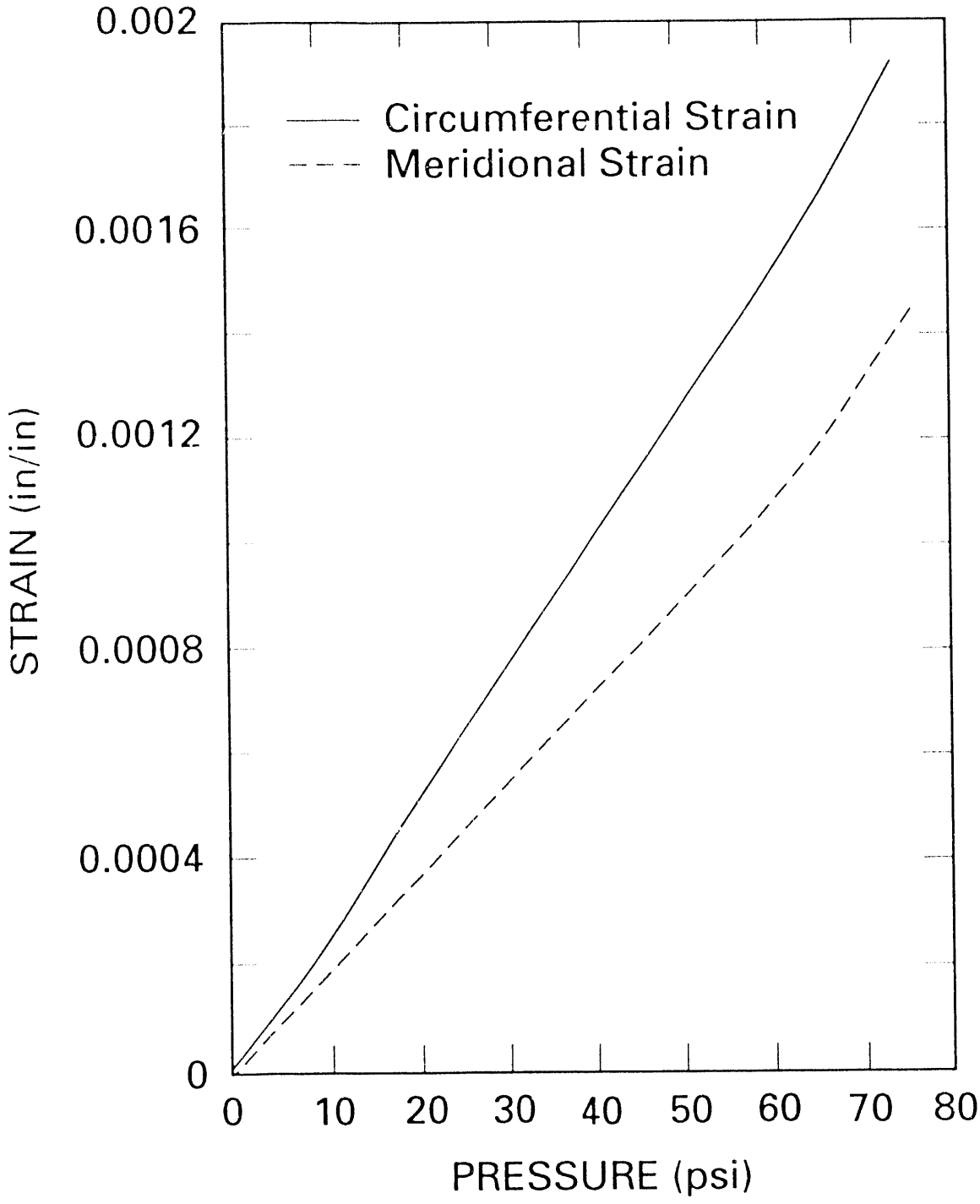

Figure 4.18 Equivalent Axial Strain-internal Pressure Relationship for Steel Containment Shell

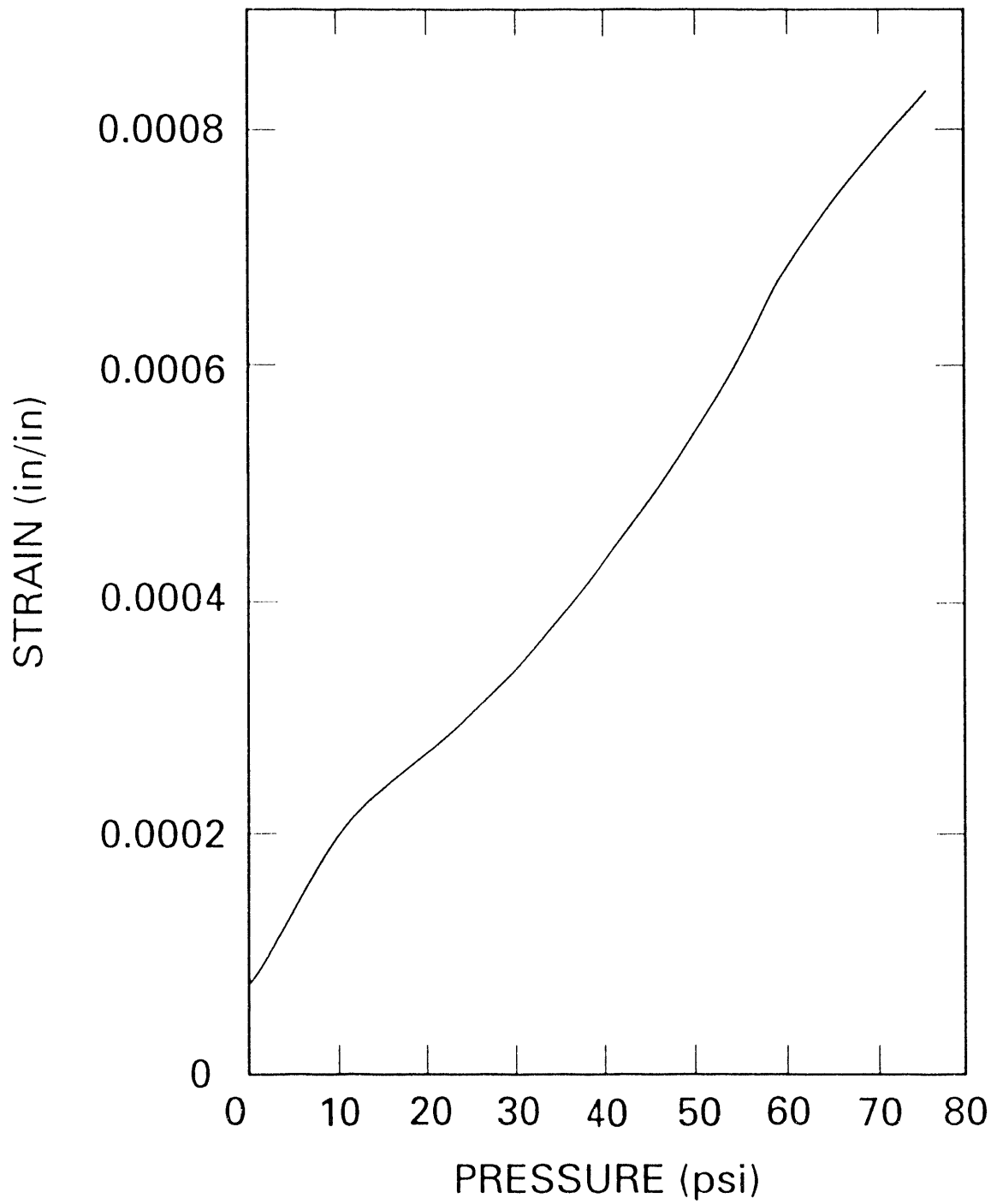

Figure 4.19 Pressure-surface Strain Relationship for the Containment Shell Near the Shell/Basemat Connection

4.5.5 Anticipated Failure Modes

Due to the non-convergence of the plasticity algorithm (see Section 4.4), the analysis was terminated at 74.123 psig. If the analysis had continued beyond this pressure, enough cracks would probably have occurred on the left outer side of the bottom ring and on the right and left of the anchor plate to form complete failure cones associated with the bottom ring and the anchor plate, respectively. If the failure cone associated with the bottom ring forms first, the anchor bolt becomes the only load path to transfer the load to the anchor plate. Hence, if the analysis could have been continued beyond this stage, one could expect failure to occur in one of two possible modes: (1) formation of a complete failure cone at the anchor plate that would result in a brittle failure; or, (2) increase in the bolt strain resulting in large deformation and a ductile failure (see discussion in Section 2).

5. SUMMARY, CONCLUSIONS AND RECOMMENDATIONS

5.1 Summary

For some time, the Containment Technology Division at Sandia National Laboratories has been conducting research to develop methods to predict pressure capacity for light water reactor containment buildings subjected to beyond design loadings. As a containment experiences large deformation during a severe accident, the containment anchorage system may deform resulting in a leakage path at the containment boundary. Current design criteria are based on simple strength of material equilibrium equations that do not account for factors such as cracking of the containment basemat or deformation of the anchor bolt and its assembly that may affect the behavior of a containment anchorage system.

A finite element analysis of the Sequoyah containment anchorage system, which considers the parameters that affect this complex system, was performed. The three dimensional model included a portion of the containment shell, knuckle plate, base plate, reinforced concrete mat, anchor bolt, anchorage system, soil foundation material, and a portion of the containment shield building. The analysis was terminated at a pressure of 74.123 psig due to numerical problems.

The analysis results showed the early formation of conical failure surfaces within the concrete that are associated with the brittle failure mode. However, these surfaces were not completely developed to the top of the containment basemat. No high strains were recorded in the anchorage system or the containment shell. Hence, failure of the containment anchorage system was not hypothesized.

5.2 Conclusions

Conclusions from this study are:

- 3-D finite element analysis of containment anchorage systems using the ABAQUS program is feasible, but the convergence problems in ABAQUS have yet to be solved.

- The size of the finite element model used in this study could be reduced by enlarging the size of the elements remote from the anchorage system. However, the convergence problem in the ABAQUS program must be addressed. Convergence should be based on a change in nodal displacements or element strains rather than residual forces. At present, this option is not available in ABAQUS.

- Failure of the weld connecting the knuckle plate to the containment shell is not likely to occur. At 74.123 psig the stresses in the weld are far below the allowable values.

- Ductile failure of the anchor bolt likely will not occur prior to the development of a complete failure cone extending from the bottom ring since the bolt will not fully be loaded until this cone forms.

- The Sequoyah containment shell near the attachment of the anchorage will remain leak tight until at least 74.123 psig. Maximum strains in

the containment shell and the containment anchorage system are well below the shell material ultimate strain.

5.3 Recommendations

Recommendations for further work are:

- Further finite element work should be done to determine the pressure at which ductile or brittle failure of the containment anchorage system occurs. Prior to continuing the analysis of the complete containment anchorage system, a simple model consisting of an anchor bolt embedded into a concrete block should be analyzed. Solutions must be carried out for both brittle and ductile failures, and the results need to be compared with experimental results.

- An experimental program is the next step to calibrate the finite element results and the current design methods. To the author's knowledge, no experimental work has been conducted to investigate the behavior of such complex anchorage systems.

APPENDIX A: SENSITIVITY STUDY OF MODELING PARAMETERS

Analytical modeling using the finite element method requires a careful consideration of all the parameters that influence the behavior of the structure being analyzed. These parameters must be identified and evaluated in order to gain an insight into the sensitivity of the results to a specific parameter.

Several parameters affect the behavior of reinforced concrete structures. These parameters include the bond between rebars and concrete and shear retention stiffness in cracked concrete. To duplicate the behavior of a reinforced concrete element, a comprehensive definition of each of these effects in an analytical model is necessary.

For proper quantification of the above listed parameters, some sort of calibration is desirable. A review of the state-of-the-art in finite element analyses involving reinforced concrete structures was conducted to identify the work done by other researchers for which experimental as well as analytical results were available. Two simple models that are related to the parameters under consideration were selected. For example, to investigate the proper idealization of bond, dowel action and aggregate interlocking, the responses of a tensile specimen and a shear wall (shown in Figures A.1 and A.2), respectively, were analyzed using the ABAQUS finite element code.

A.1 Bond Idealization

While link elements have been commonly used for idealizing bond behavior, the tension stiffening concept was selected for its ease of application and aid to solution convergence. Tension stiffening is incorporated in the concrete material model in ABAQUS by expressing the retained tensile stress (beyond concrete tensile strength) as a linearly decreasing function of strain normal to the cracks. Three different values for the maximum strain, ϵ_y, $10\epsilon_{cr}$ and $3\epsilon_y$ (see curves A, B and C, Figure A.3), were used to investigate the behavior of the tension member shown in Figure A.1. These values were suggested in [28, 29] respectively. An analysis with no tension stiffening was also conducted. A quarter-symmetry model was used for idealizing the tension member. Solid elements (C3D8 in ABAQUS) were used to model the concrete while two dimensional truss elements (C1D2 in ABAQUS) were employed for the rebar idealization. Symmetry boundary conditions were imposed on the symmetry planes. An axial load was applied in increments at the end face of the rebar, and a sufficient number of iterations within each load increment were allowed to ensure convergence.

Figure A.4 illustrates steel stress versus displacement at the end face of the rebar. The analysis with no tension stiffening resulted in a cracking load lower than the experimental and analytical results documented in [30, 31]. Although Curve C gives results closer to the experimental results, it cannot be used in analysis because a value of maximum strain greater than the yield strain of the reinforcement would artificially increase the total stress in the direction of any yielded reinforcement [28]. Tension stiffening as represented by Curves A and B yielded results bounded by Curve C and no tension stiffening results. The tension stress-strain relation given by Curve B was selected to model bond in the analysis of the Sequoyah Anchorage System.

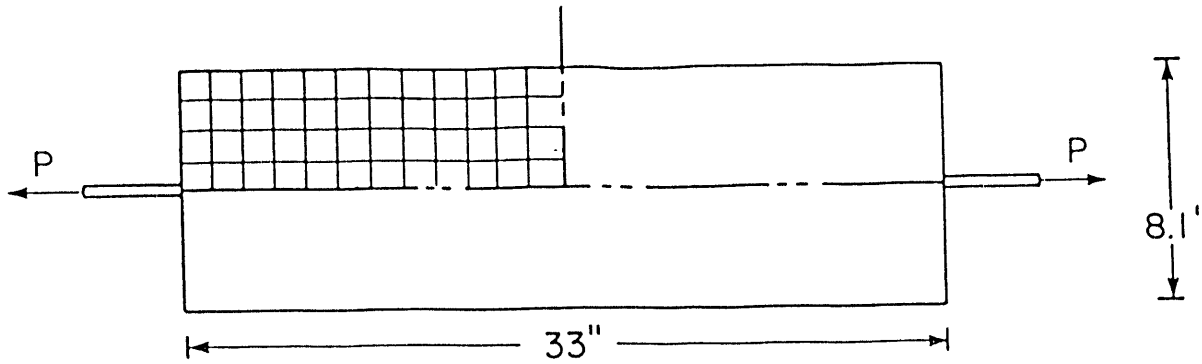

Figure A.1 Tension Member Used to Investigate Bond Idealization

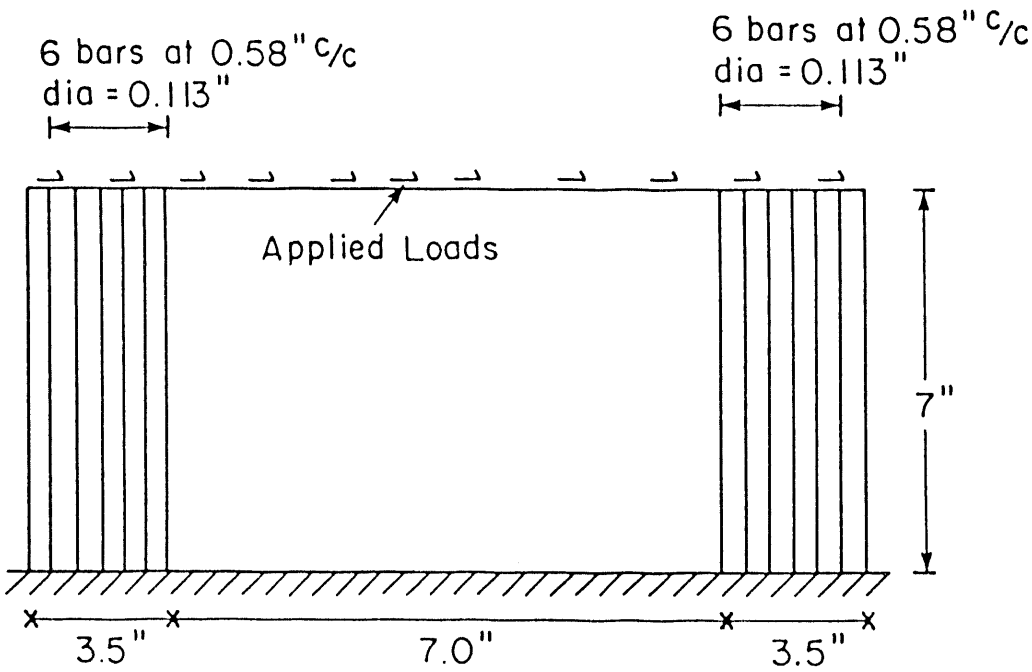

Figure A.2 Shear Wall Used to Investigate Shear Transfer in Reinforced Concrete Structures

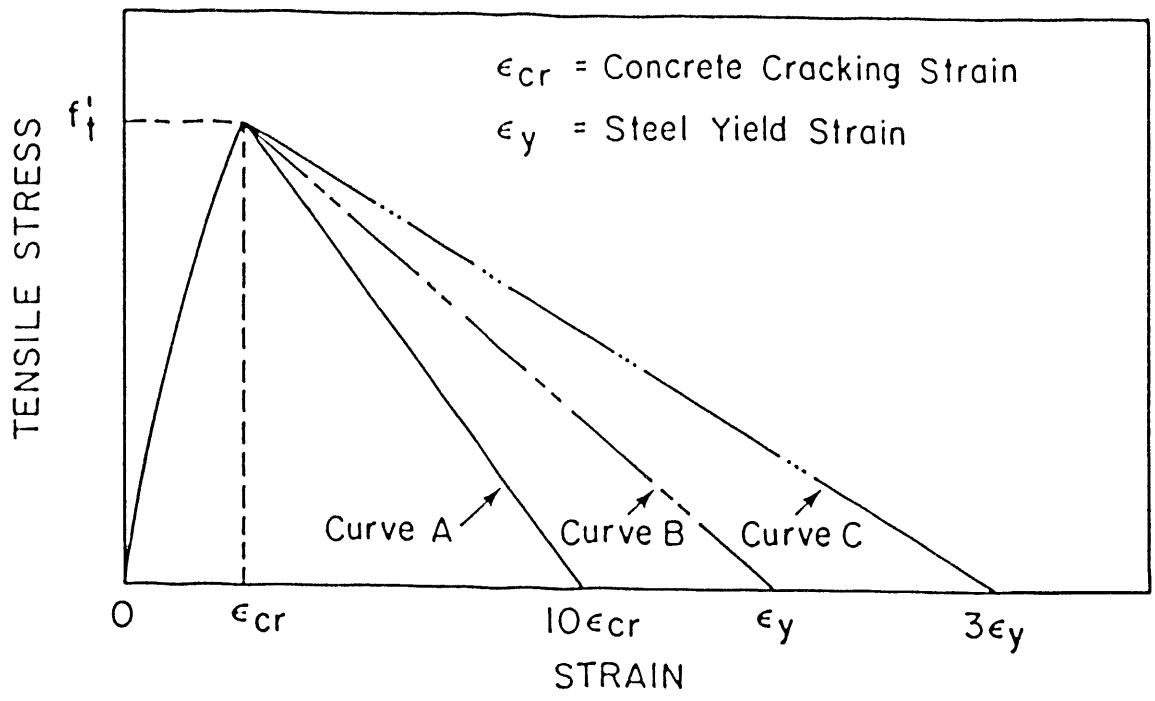

Figure A.3 Different Relationships Used to Investigate Tension Stiffening in Reinforced Concrete Structures

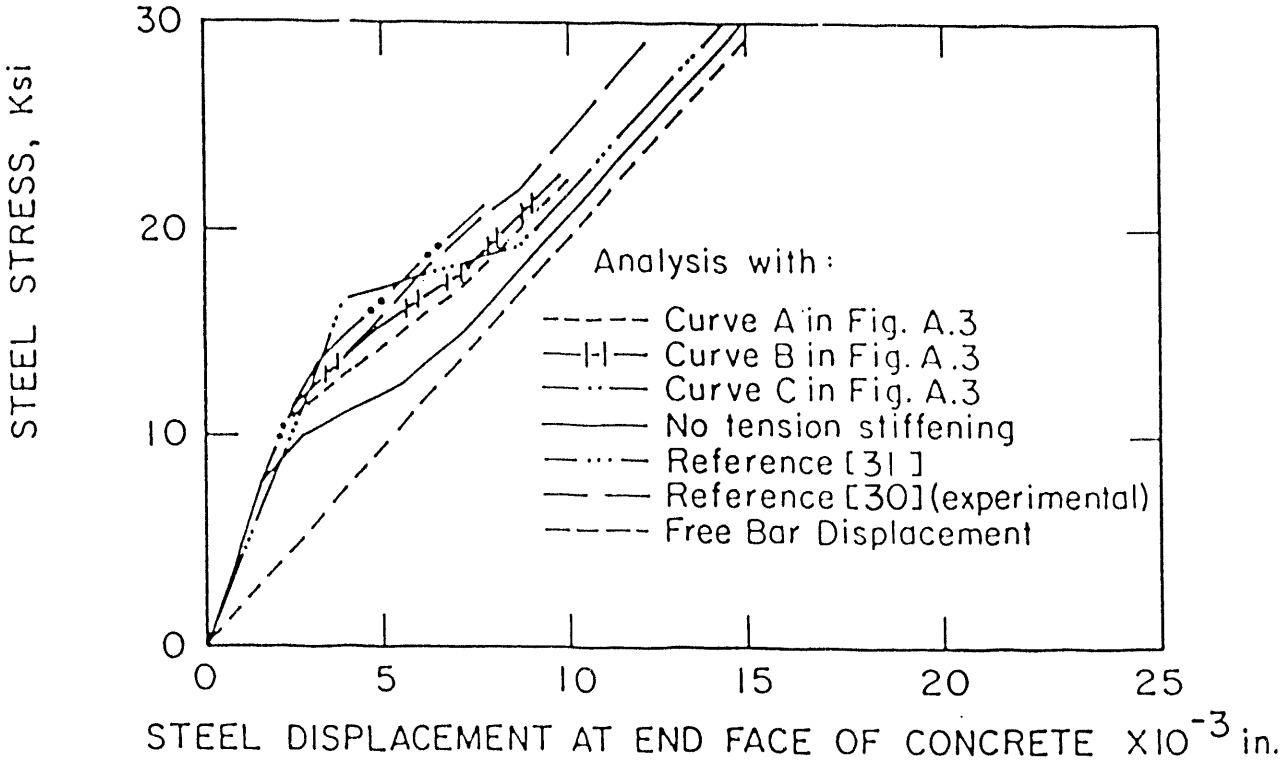

Figure A.4 Stress-displacement Curves for the Tension Member in Figure A.1

A.2 Dowel Action and Aggregate Interlocking

To verify the adequacy of the results summarized above and to study dowel action and aggregate interlocking, which cannot be studied in a tension member, a shear wall, that was tested and analyzed by Al-Mahaiidi [20], (see Figure A.2) was investigated.

Dowel action and aggregate interlocking are incorporated into the finite element analysis by using a reduced shear modulus G_1, in the material matrix (see Section 3.2 of this report). Al-Mahaiidi [20] developed hyperbolic expressions relating the elastic shear modulus of uncracked concrete, G, to the reduced shear stiffness G_1 of cracked concrete. These expressions are:

$$G_1 = 0.4G/(\epsilon_1/\epsilon_0) \qquad \text{for } \epsilon_1 > \epsilon_0 \tag{A.1}$$

$$G_1 = G \qquad \text{for } \epsilon_1 < \epsilon_0 \tag{A.2}$$

where ϵ_1 is the principal tensile strain normal to the crack, ϵ_0 is the concrete cracking tensile strain, and G is the elastic shear modulus of uncracked concrete. The shear modulus-strain relationship used herein is shown in Figure A.5.

At the beginning of this project, the ABAQUS Version 4.5.165 was used. This version allowed the user to specify a piecewise shear modulus strain relationship. The relationship given in Equations A.1 and A.2 were used in conjunction with this version to analyze the shear wall shown in Figure A.2.

The analysis of the shear wall was also accomplished using ABAQUS Version 4.7.19. In this version, the shear modulus, G_1, for cracked concrete is reduced linearly to zero as the crack opening increases:

$$G_1 = G\,(1 - \epsilon_1/\epsilon_{max}) \tag{A.3}$$

where ϵ_{max} is a user specified strain value beyond which the shear modulus becomes zero. In this work, ϵ_{max}, was selected equal to the rebar yield strain. The shear modulus-strain relationship obtained from Equation A.3 is illustrated in Figure A.5.

In modeling the shear wall problem, solid elements (C3D8 in ABAQUS) were used to idealize the concrete while truss elements (C1D2 in ABAQUS) were used to idealize the reinforcing bars. Symmetry boundary conditions along the vertical plane through the wall thickness were imposed. The finite element model is shown in Figure A.6. The six layers of reinforcement at each side of the panel were represented by two layers consisting of 14 elements as shown by the heavy lines in Figure A.6. Bond behavior was incorporated by the tension stiffening approach outlined in Section A.1. Horizontal loads were applied in small increments at the top nodes in the model.

Figure A.7 illustrates the load-displacement relationship obtained from two analyses with different tension stiffening curves (Curves A and B in Figure A.3). This displacement is illustrated for the top right corner of the wall in

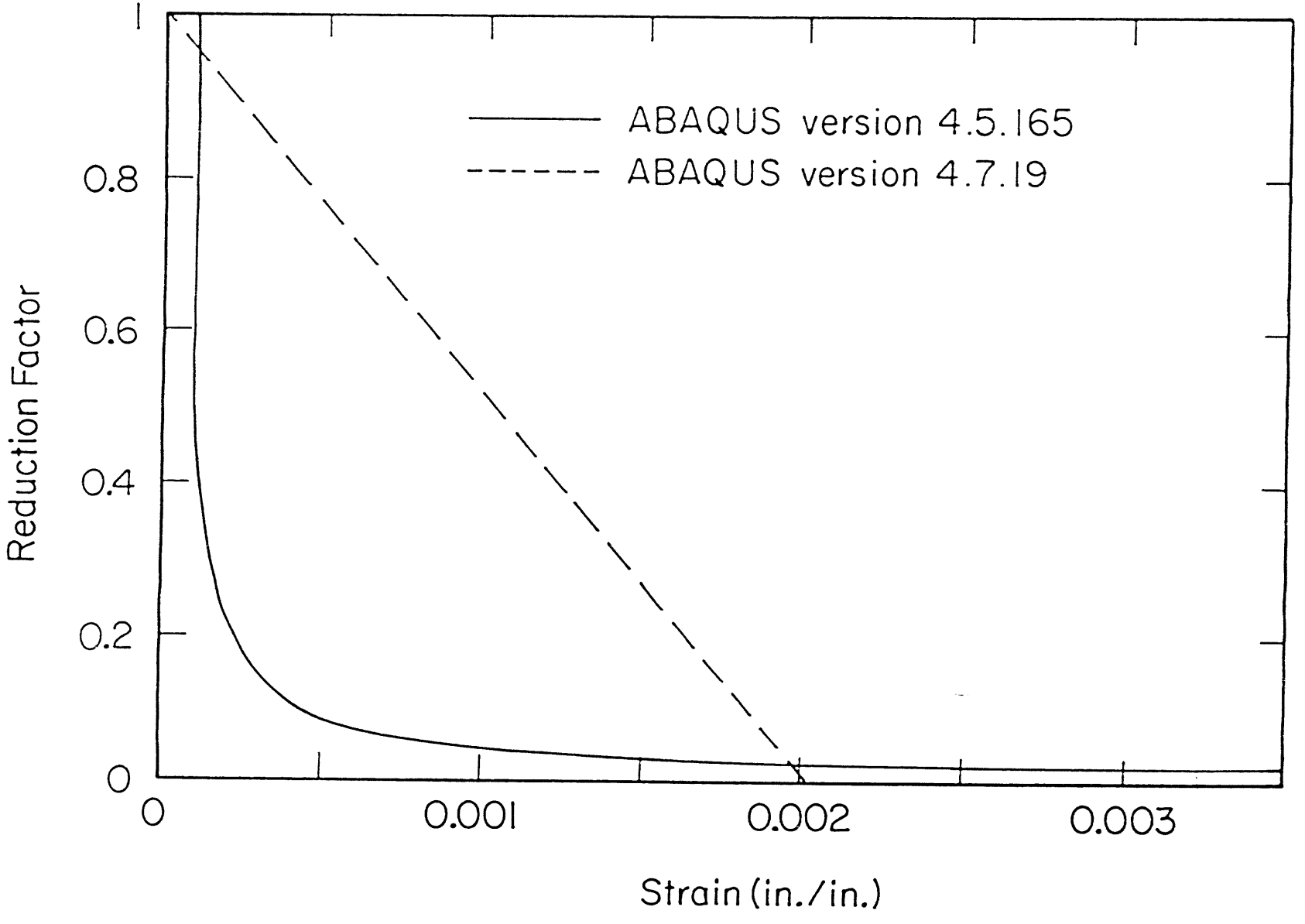

Figure A.5 Shear Modules-strain Relationship Used to Analyze the Shear Wall in Figure A.2

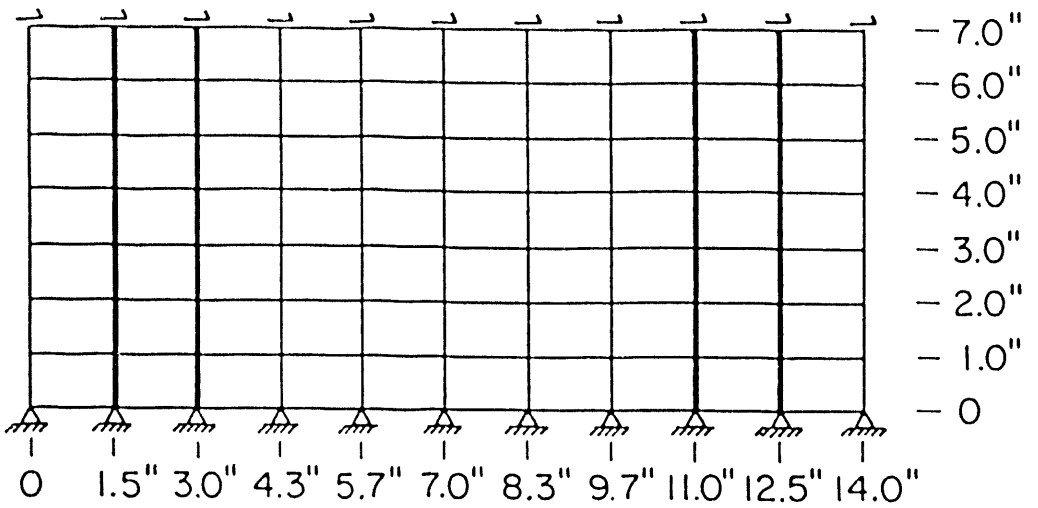

Figure A.6 Finite Element Mesh for the Shear Wall in Figure A.2

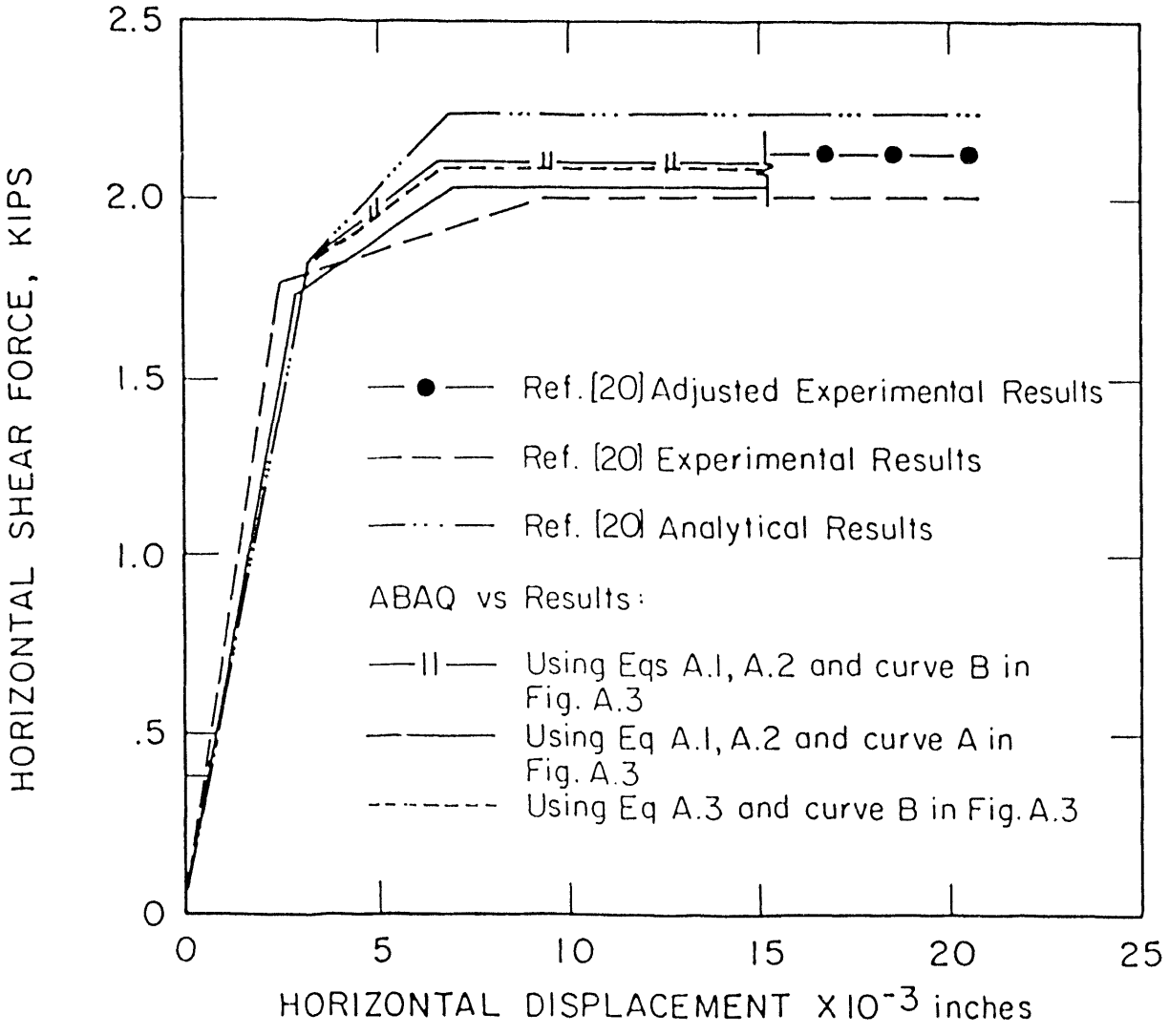

Figure A.7 Load-Displacement Relationship for the Top Right Corner of the Shear Wall in Figure A.2

Figure A.5. Also shown are the experimental and analytical results given in [20]. Al-Mahaiidi [20] adjusted the experimental result to reflect the effects of true fixity at the base, which was not duplicated in the experiment. As can be seen, the results obtained by using curve B for tension stiffening in conjunction with the shear retension option in the ABAQUS program using Equations A.1 and A.2 or A.3 yielded results closer to the adjusted experimental results.

A.3 Conclusions

Based on the sensitivity studies summarized in Appendix A, the tension stiffening relation defined by Curve B in Figure A.2 was chosen to model the bond between rebars and plain concrete. The shear retention curve given by Equation A.3 was used to represent aggregate interlock and dowel action in the analytical model for the containment anchorage system.

REFERENCES

[1] Bridges, T.L., "Containment Penetration Elastomer Seal Leak Tests," NUREG/CR-4944, SAND87-7118, Sandia National Laboratories, Albuquerque, NM (July 1987).

[2] Clauss, D.B., "Severe Accident Testing of Electrical Penetration Assemblies," NUREG/CR-5334, SAND89-0327, Sandia National Laboratories, Albuquerque, NM (Nov 1989).

[3] Parks, M.B., "Evaluation of the Leakage Behavior of Inflatable Seals Subjected to Severe Accident Conditions," NUREG/CR-5394, SAND89-1454, Sandia National Laboratories, Albuquerque, NM (Nov 1989).

[4] Brinson, D.A. and Groves, G.H., "Evaluation of Seals for Mechanical Penetrations of Containment Buildings," NUREG/CR-5096, SAND88-7016, Sandia National Laboratories, Albuquerque, NM (Aug 1988).

[5] Miller, J.D., "Analysis of Shell-Rupture Failure Due to Hypothetical Elevated Temperature Pressurization of the Sequoyah Unit 1 Steel Containment Building," NUREG/CR-5405, SAND89-1650, Sandia National Laboratories, Albuquerque, NM (Feb 1990).

[6] Greimann, L.F., Fanous, F., Rogers, J., and Bluhm, D., "An Evaluation of the Effects of Design Details on the Capacity of LWR Steel Containment Buildings," NUREG/CR-4870, SAN87-7066, Sandia National Laboratories, Albuquerque, NM (May 1987).

[7] ACI Committee 349, "Code Requirements for Nuclear Safety Related Concrete Structures (ACI 349-80)," ACI Manual of Concrete Practice, Part 4 (1985).

[8] Lynch, T.J. and Burdette, E.G., "Some Design Consideration for Anchors in Concrete," A.C.I., pp 91-97 (1991).

[9] Letter from D. Clauss, Sandia National Laboratories to L. Greimann, Ames Laboratory, 6442 File 1709.071, (Feb 1989).

[10] "Sequoyah Nuclear Plant - Concrete Structural Slab," Tennessee Valley Authority, Drawing Nos. 41N708-1, 41N708-2, 41N700-1 and 41N710-2.

[11] ABAQUS, "USER's and Theoretical Manuals," Hibbitt, Karlsson & Sorensen, Inc., Version 4.7.

[12] Gerstal, K., et al., "Modeling of Reinforcement and Representation of Bond," Finite Element Analysis of Reinforced Concrete, State-of-the-Art Report, A.S.C.E., pp. 149-203 (1982).

[13] Shiro, M. and Fujii, S., "Bond-Slip Models in Finite Element Analysis," Proceedings of the Seminar sponsored by the Japan Society for the Promotion of Science and the U.S. National Science Foundation, Tokyo, Japan, A.S.C.E., pp. 348-363 (May 1985).

[14] Gilbert, R.I. and Warner, R.F., "Nonlinear Analysis of Reinforced Concrete Slabs with Tension Stiffening," Report No. R-167, University of South Wales, Kensington, Australia (1978).

[15] Gilbert, R.I. and Warner, R.F., "Tension Stiffening in Reinforced Concrete Slabs," Journal of Structural Division, A.S.C.E., Vol. 104, pp. 1885-1900 (Dec 1978).

[16] Telephone conversation between Mr. Luis Resende from Hibbitt, Karlsson and Sorensen, Inc., and F. Fanous from Ames Laboratory, Iowa State University (Feb 1989).

[17] "Kanott, Y., et Al., "Shear Mechanism of Reinforced Concrete Members," Proceedings of the Seminar sponsored by the Japan Society for the Promotion of Science and the U.S. National Science Foundation, Tokyo, Japan, A.S.C.E., pp. 308-328 (May 1985).

[18] Cedolin, L., et al., "Shear Transfer," Finite Element Analysis of Reinforced Concrete, State-of-the-Art Report, A.S.C.E., pp. 234-308 (1982).

[19] Cedolin, L. and Dei Poli, S., "Finite Element Studies of Shear Critical Reinforced Concrete Beam," Journal of the Engineering Mechanics Division, A.S.C.E., Vol. 103, No. EM3 (Jun 1977).

[20] Al-Mahaiidi, R., "Nonlinear Finite Element Analysis of Reinforced Concrete Deep Member," Report No. 79-1, Department of Structural Engineering, Cornell University (1979).

[21] Timoshenko, S. and Woinowsky-Krieger, S., Theory of Plates and Shells, McGraw-Hill: New York (1959).

[22] "PATRAN-Mechanical Computer Aided Engineering Software Interface System," Developed by PDA Engineering, California, USA (1987).

[23] Park, R. and Paulay, T., Reinforced Concrete Structures, John Wiley & Sons: New York, pp. 12-13 (1975).

[24] Greimann, L.F., "Sequoyah Containment Performance Analysis for Severe Accident Loading," Progress Report, submitted to D. Clauss, Sandia National Laboratories, Ames Laboratory Project No. 66962 (Aug 1987).

[25] Telephone conversations and letters between Luis Resende from Hibbitt, Karlsson and Sorenson, Inc. and F. Fanous from Ames Laboratory (Aug 1989).

[26] Telephone conversation between Paul Sorenson from Hibbitt, Karlsson and Sorenson, Inc. and F. Fanous from Ames Laboratory (Jan 1990).

[27] Telephone conversation between B. Parks from Sandia National Laboratories and F. Fanous from Ames Laboratory (Feb 1990).

[28] Schnobrich, W.C., "The Role of Finite Element Analysis of Reinforced Concrete Structures," Finite Element Analysis of Concrete Structures, A.S.C.E., Edited by Christian Mayer and Hajime Okamura, Tokyo, Japan, pp. 1-14 (1986).

[29] Weatherby, J.R., "Axisymmetric Analysis of a 1:6-Scale Reinforced Concrete Containment Building Using a Distributed Cracking Model for the Concrete," NUREG/CR-4969, SAND87-1670, Sandia National Laboratories, Albuquerque, NM (Sept 1987).

[30] Houde, J., "Study of Force-Displacement Relationships for the Finite Element Analysis of Reinforced Concrete," Report No. 73-2, Department of Engineering and Applied Mechanics, McGill University, Montreal, Canada (1973).

[31] Khouzan, M., "A Finite Element Investigation of Reinforced Concrete Beams," M.S. Thesis, Department of Engineering and Applied Mechanics, McGill University, Montreal, Canada (1977).

DISTRIBUTION:

Richard N. White
54 Sunny Slope Road
Ithaca, NY 14850

James F. Costello
RES/SSEB, NL/S-217A
U.S. Nuclear Regulatory Commission
Washington, DC 20555
(10 Copies)

D. Bluhm
Ames Laboratory
Iowa State University
Department of Civil Engineering
423 Town Engineering Bldg.
Ames, IA 50011
(20 Copies)

Fouad Fanous
Ames Laboratory
Iowa State University
Department of Civil Engineering
423 Town Engineering Bldg.
Ames, IA 50011

Lowell Greimann
Ames Laboratory
Iowa State University
Department of Civil Engineering
420 Town Engineering Bldg.
Ames, IA 50011-2322

Mete A. Sozen
University of Illinois
Department of Civil Engineering
205 N. Mathews Ave.
Urbana, IL. 61801-2397

Richard N. White
Cornell University
School of Civil & Environ. Engr.
Hollister Hall
Ithaca, NY 14853

Thomas J. Ahl
CBI Technical Services Co.
800 Jorie Boulevard
Oak Brook, IL 60521

Brian A. Erler
Sargent & Lundy Engineers
55 East Monroe Street
Chicago, IL 60603

Lyle D. Gerdes
ABB-Combustion Engineering, Inc.
ABB-Combustion Engineering Nuclear Power
P. O. Box 500, 1000 Prospect Hill Rd.
Windsor, CT 06095-0500

Theodore E. Johnson
Bechtel Savanah River, Inc.
802 E. Martintown Road
North Augusta, SC 29841

Richard S. Orr
Westinghouse Electric Corporation
Nuclear & Adv. Tech Div.
MS 4-28
P. O. Box 355
Pittsburgh, PA 15230-0355

Bertold W. Pfeifer
Bechtel Power Corp.
12440 E. Imperial Hwy.
Norwalk, CA 90650-2550

John D. Stevenson
Stevenson & Associates
9217 Midwest Avenue
Cleveland OH 44125

H. T. Tang
Electric Power Research Institute
3412 Hillview Avenue
P. O. Box 10412
Palo Alto, CA 94303

Harold Townsend
General Electric Company
ABWR Programs
175 Curtner Avenue (MC-754)
San Jose, CA 95125

Joseph J. Ucciferro
United Engineers & Constructors, Inc.
% Philadelphia Electric
MS 62C-3
965 Chesterbrook Blvd.
Wayne, PA 19087

Internal SNL:
6400 N. R. Ortiz
6403 W. A. von Riesemann
6449 M. P. Bohn
6449 L. D. Lambert
6449 J. S. Ludwigsen
6449 M. B. Parks (10)
6449 D. W. Pace
6449 B. L. Spletzer
6449 R. A. Watson
7141 Technical Library (5)
7151 Technical Publications (1)
8523-2 Central Technical Files (1)

☆ U.S. GOVERNMENT PRINTING OFFICE 1992—774-122/80072

END

DATE
FILMED
3/30/94